Workshop: electron crystallography

Basel, August 4

Carsten Sachse

EMBL

EMBL

Single-particle cryo-EM of the machinery involved in abnormal protein aggregation

www.embl.de/research/units/scb/sachse

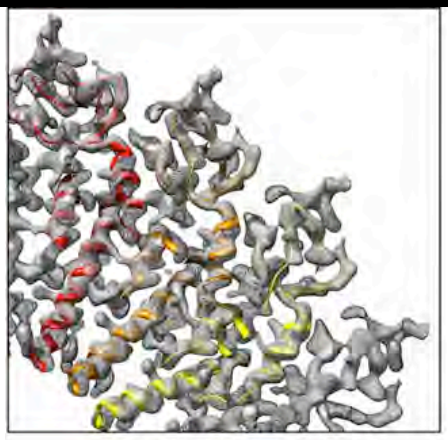

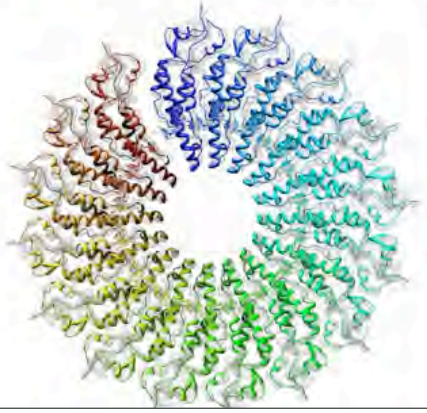

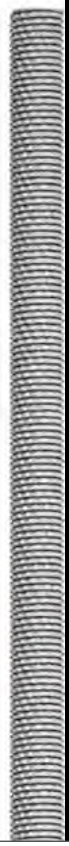

Structure of an Aβ amyloid fibril

Structure of Tobacco Mosaic Virus

Reprinted from COLD SPRING HARBOR SYMPOSIA ON QUANTITATIVE BIOLOGY
Volume XXXVI, 1971
Printed in U.S.A.

Three-dimensional Image Reconstructions of Some Small Spherical Viruses

R. A. CROWTHER AND LINDA A. AMOS
Medical Research Council, Laboratory of Molecular Biology, Cambridge, England

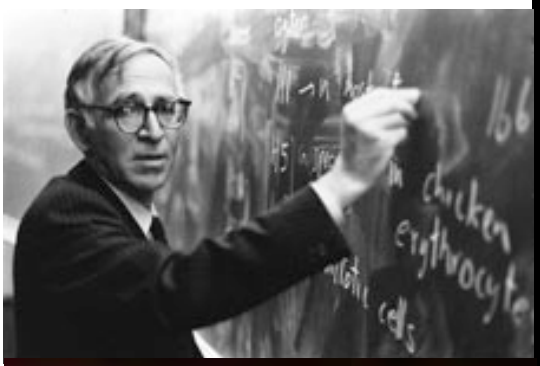

130 NATURE, VOL. 217, JANUARY 13, 1968

Reconstruction of Three Dimensional Structures from Electron Micrographs

by
D. J. DE ROSIER
A. KLUG
MRC Laboratory of Molecular Biology, Hills Road, Cambridge

General principles are formulated for the objective reconstruction of a three dimensional object from a set of electron microscope images. These principles are applied to the calculation of a three dimensional density map of the tail of bacteriophage T4.

New Scientist 30 July 1970

3-D objects from an EM image

With the aid of a computer, a Cambridge team have devised a powerful technique for reconstructing three-dimensional objects from two-dimensional photographs taken in the electron microscope. The technique promises to revolutionize the study of biological structures. Here one of the team describes its first results as applied to spherical viruses

Sample arrangements in cryo-EM

Single particles **Icosahedral** **Helical crystal** **2D crystal**

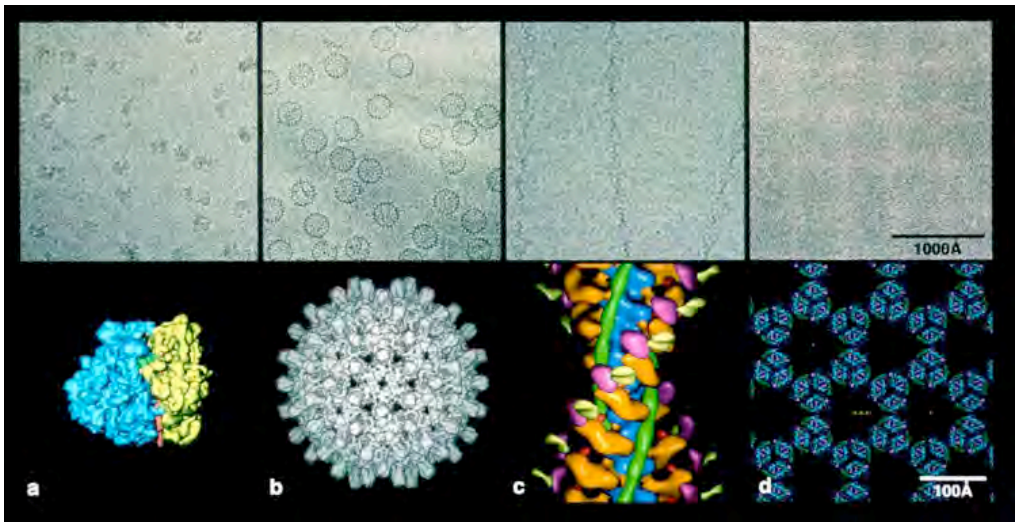

Ribosome Hepatitis B Virus Actin-Myosin Aquaporin

Baker & Henderson (2001) Int.Tab.Cryst.Vol.F

Fourier theory 2D

- Basics of image processing

  Real space, Fourier space, convolution, lattice lines, correlation, autocorrelation

- Image formation

  Contrast transfer function and application

Basics of image processing: Fourier transform

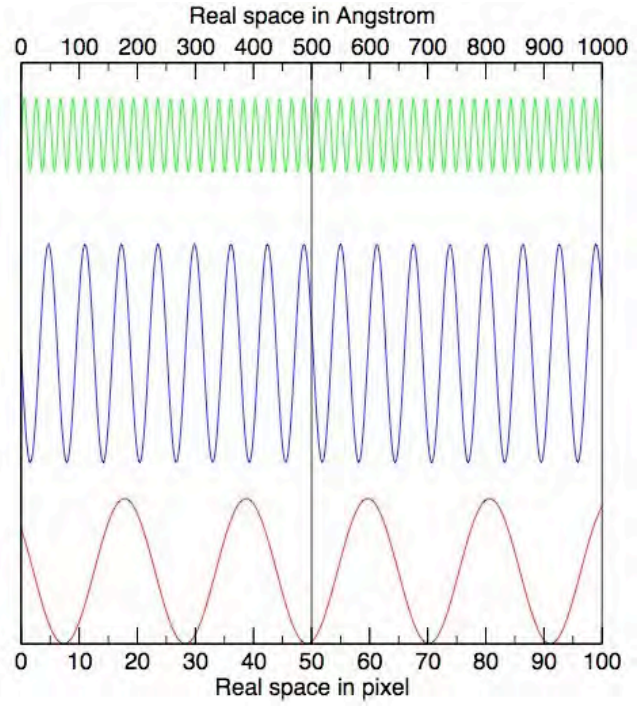

3 Cosine functions

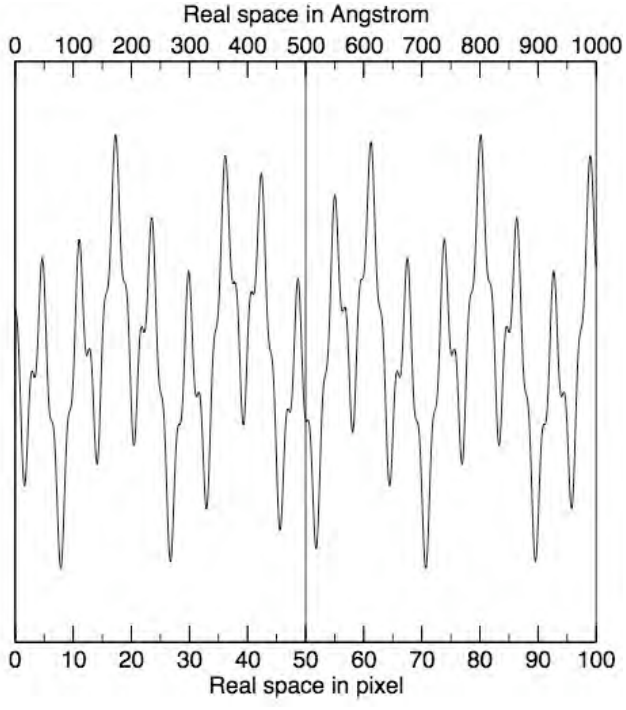

Real-space 1D image as a superposition of 3 cosine functions

Basics of image processing: Fourier transform

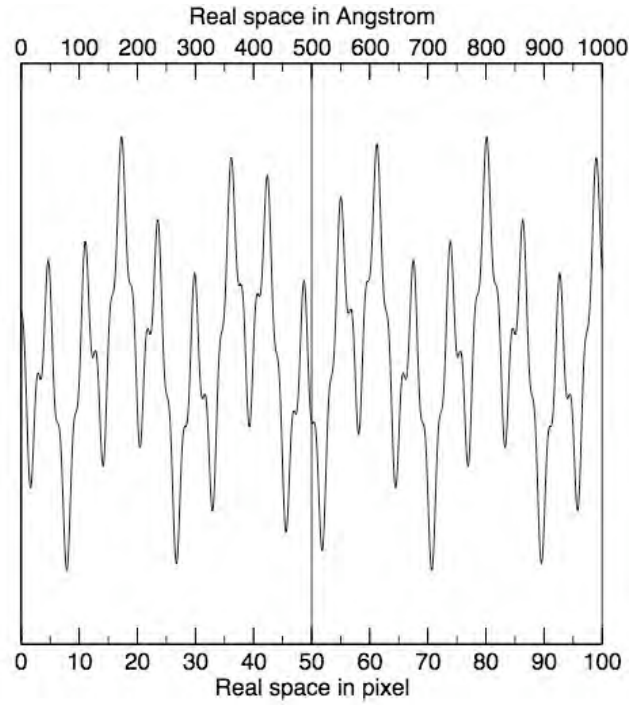

FT

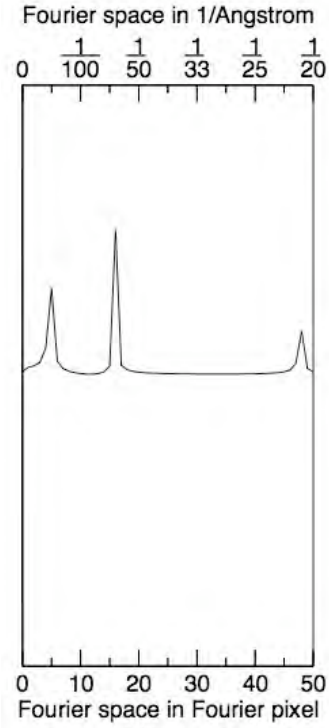

Real-space 1D image

3 Fourier peaks

Basics of image processing: Fourier transform

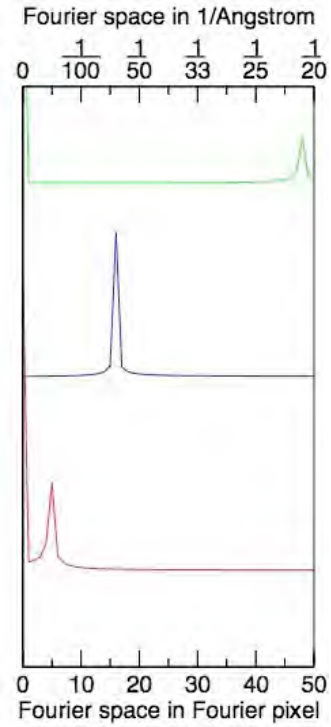

FT

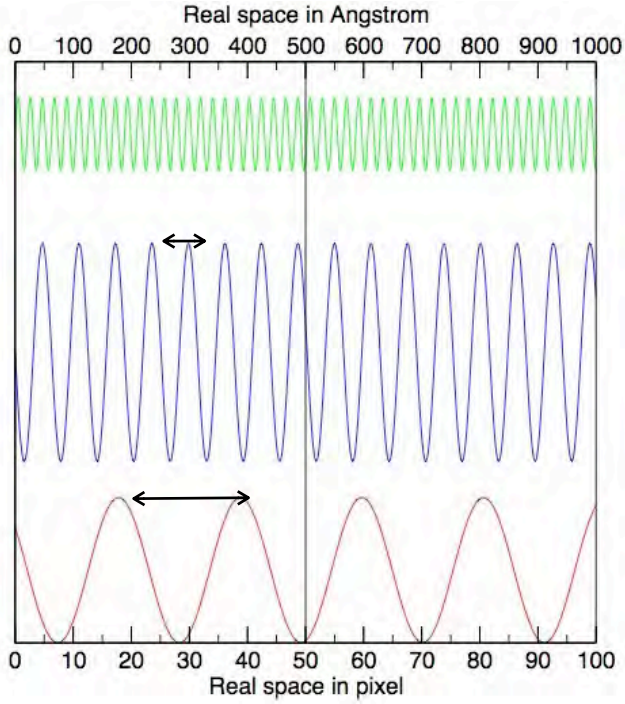

3 Fourier components

3 cosine functions are characterized by different frequencies

Basics of image processing: Fourier transform

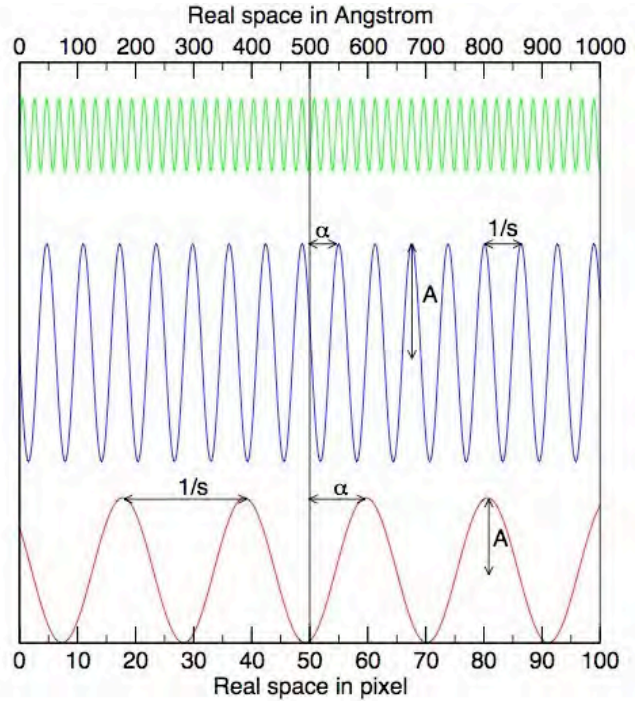

3 cosine functions are characterized by frequencies, amplitudes and phases

1. 1/s

Frequency tells you about image spacings

2. A

Amplitude tells you “how much” of a frequency component is present

3. α

Phase tells you “where” the frequency components are located in the image

Basics of image processing: Fourier transforms of 2D images

Russ, The Image Processing Handbook, 2007

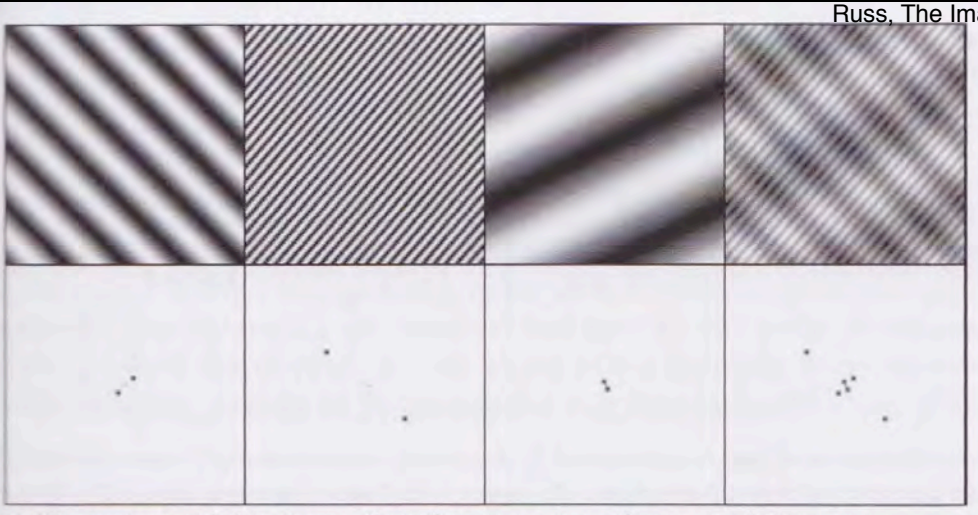

6.5 *Three sinusoidal patterns, their frequency transforms, and their sum.*

Real space

Fourier space

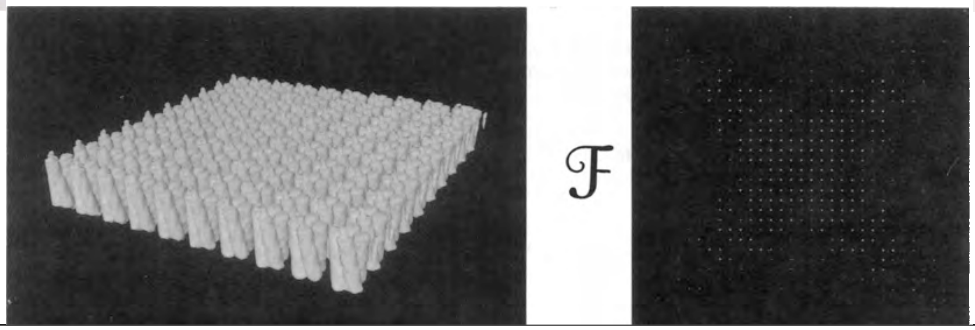

Chiu et al. Biophysical Journal (1993) vol. 64 (5) pp. 1610-25

Basics of image processing: image sampling and quantization

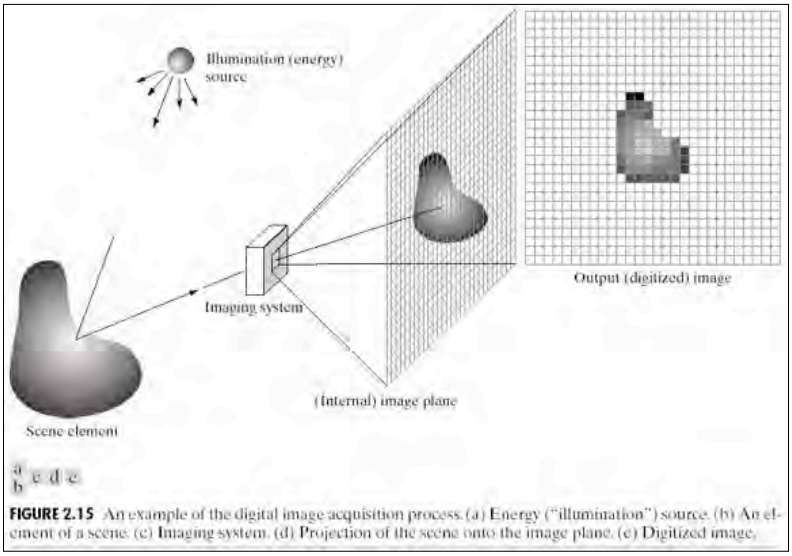

FIGURE 2.15 An example of the digital image acquisition process. (a) Energy ("illumination") source. (b) An element of a scene. (c) Imaging system. (d) Projection of the scene onto the image plane. (e) Digitized image.

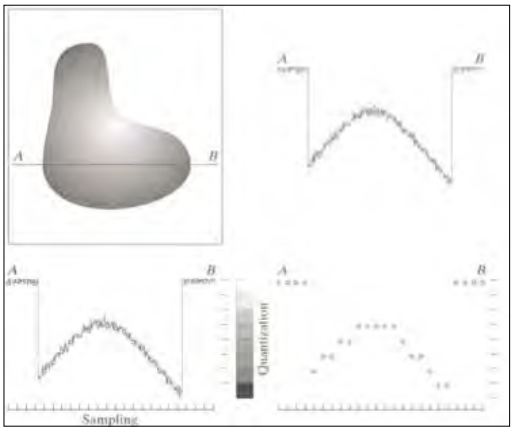

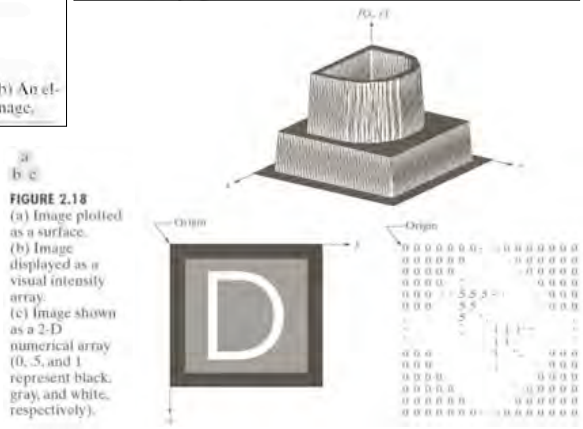

FIGURE 2.18
(a) Image plotted as a surface.
(b) Image displayed as a visual intensity array.
(c) Image shown as a 2-D numerical array (0, .5, and 1 represent black, gray, and white, respectively).

Gonzales and Woods, Digital Image Processing, 2008

Basics of image processing: discrete Fourier transforms

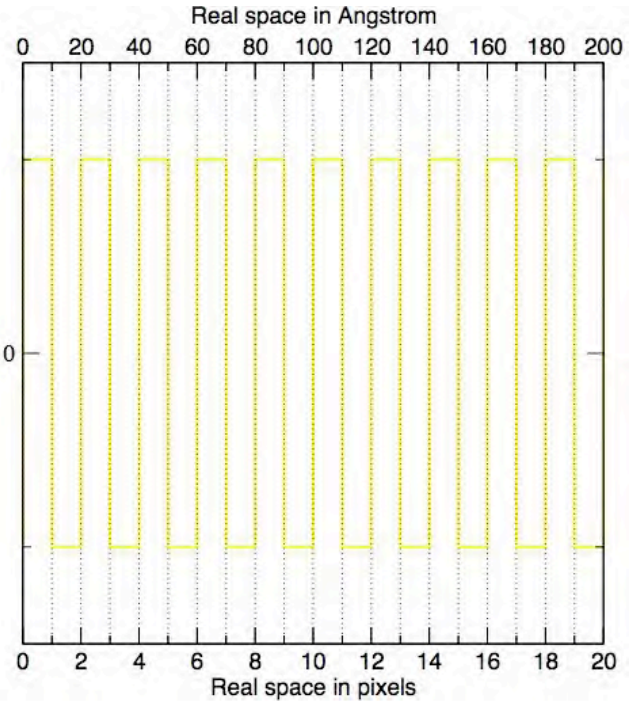

FT

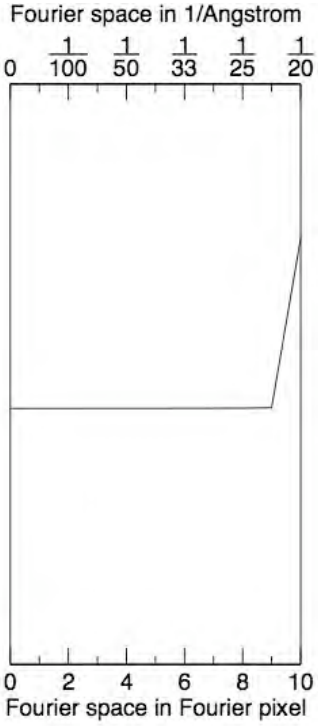

cosine fct. with maximum frequency on a discrete grid

pixelsize = 200Å/20pix = 10 Å/pix

peak at maximum spatial frequency=Nyquist

Basics of image processing: discrete pixel images can give rise to aliasing

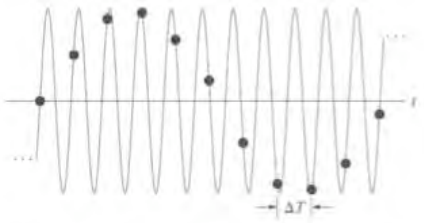

FIGURE 4.10 Illustration of aliasing. The under-sampled function (black dots) looks like a sine wave having a frequency much lower than the frequency of the continuous signal. The period of the sine wave is 2 s, so the zero crossings of the horizontal axis occur every second. ΔT is the separation between samples.

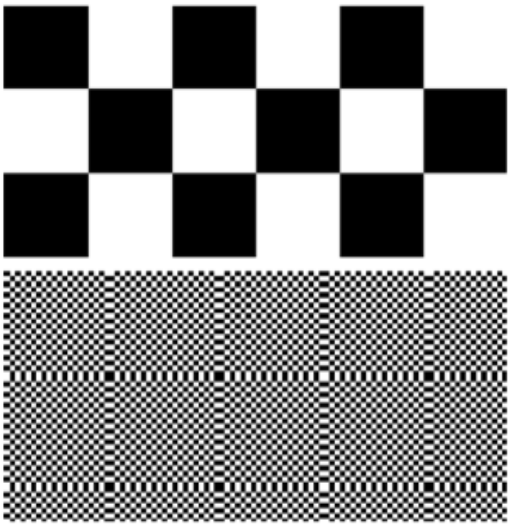

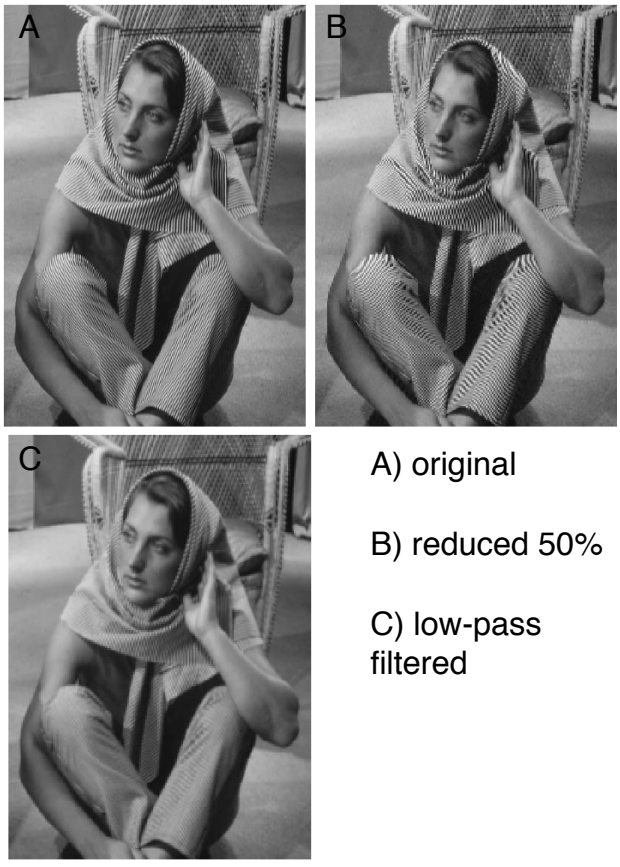

A) original

B) reduced 50%

C) low-pass filtered

Basics of image processing: properties of discrete 2D Fourier transforms

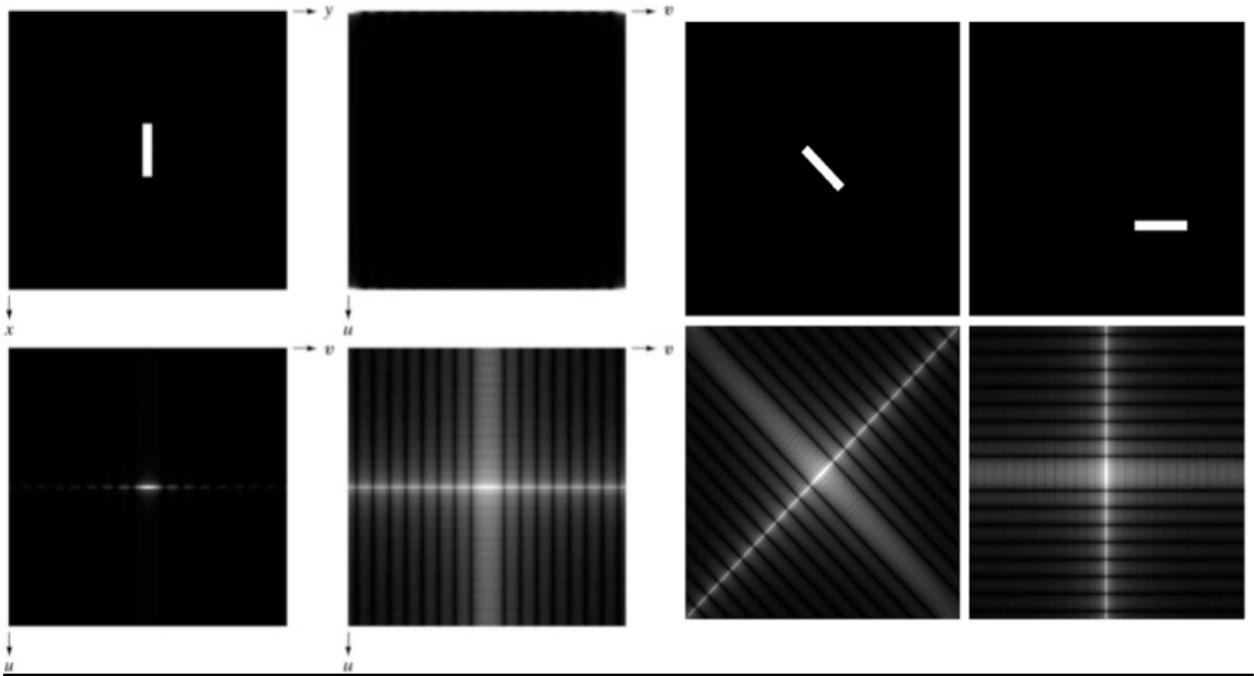

binary rectangle	power spectrum not centered	rectangle rotated by 45º	rectangle rotated by 90º and translated
power spectrum (ps)	ps intensities log transformed	ps rotated by 45º	ps rotated by 90º

Gonzales and Woods, Digital Image Processing, 2008

Basics of image processing: Fourier transforms of 2D images

Russ, The Image Processing Handbook, 2007

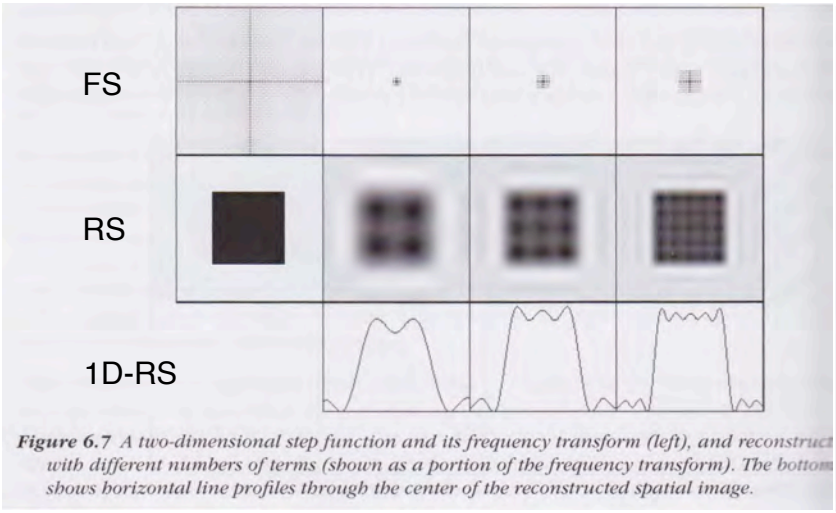

Figure 6.7 A two-dimensional step function and its frequency transform (left), and reconstruct with different numbers of terms (shown as a portion of the frequency transform). The bottom shows horizontal line profiles through the center of the reconstructed spatial image.

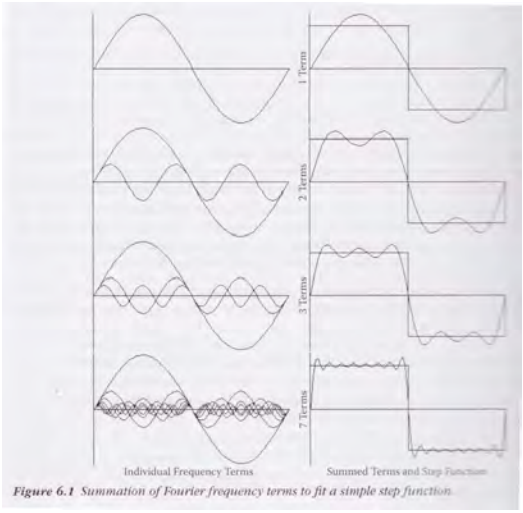

Figure 6.1 Summation of Fourier frequency terms to fit a simple step function.

Density steps in real space introduce artifacts during image processing (e.g. low-pass filtration)
Solution: addition of smooth falloff ramps to edges (RS), e.g. cosine falloff

Basics of image processing: Fourier transforms of 2D images

Fourier space

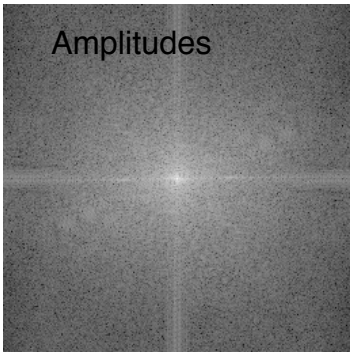

FT

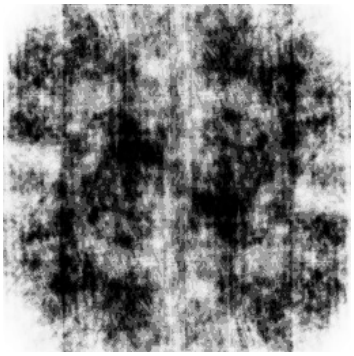

FT

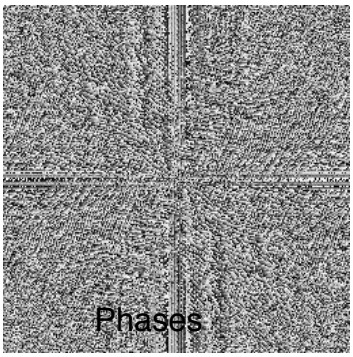

Phase information dominates image perception

Real space

http://homepages.inf.ed.ac.uk/rbf/HIPR2/fourier.htm

Basics of image processing: Fourier transforms of 2D images

Amplitudes

FT → iFT →

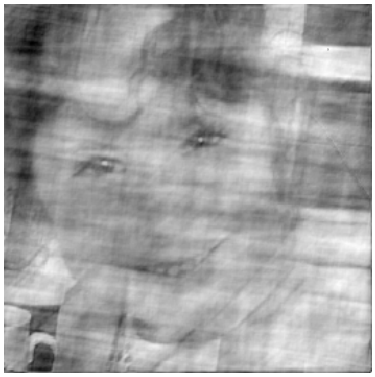

Phases

Phase information dominates image perception

http://homepages.inf.ed.ac.uk/rbf/CVonline/LOCAL_COPIES/OWENS/LECT4/node2.html

Basics of image processing: Fourier filters of images

Real -->Fourier -->Real

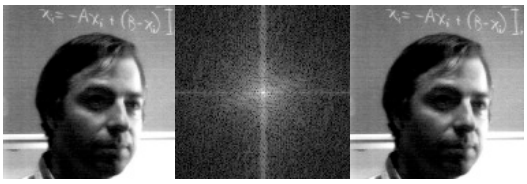

Low-pass filter

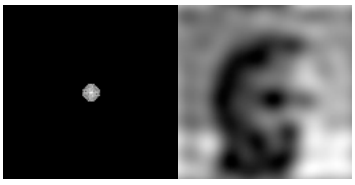

High-pass filter

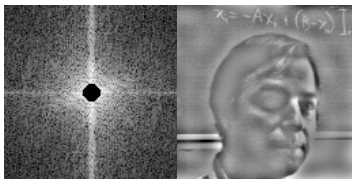

Band-pass

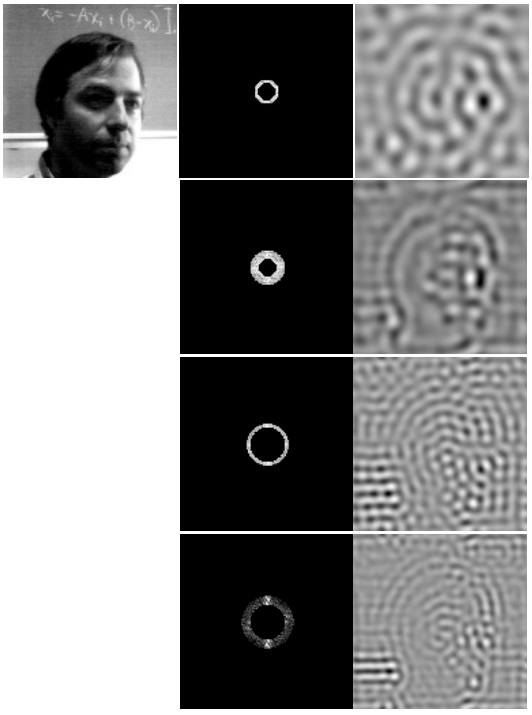

http://sharp.bu.edu/~slehar/fourier/fourier.html

Basics of image processing: Fourier filters of images

Real -->Fourier -->Real

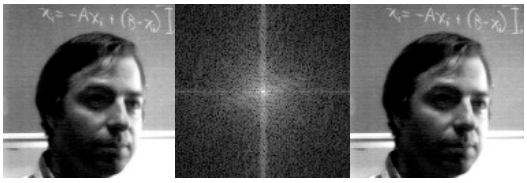

Low-pass filter

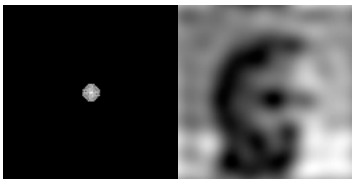

Gaussian low-pass filter

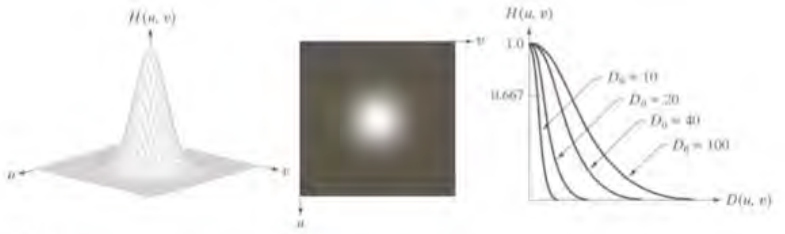

a b c

FIGURE 4.47 (a) Perspective plot of a GLPF transfer function. (b) Filter displayed as an image. (c) Filter radial cross sections for various values of D_0.

a b c

FIGURE 4.40 (a) Perspective plot of an ideal lowpass-filter transfer function. (b) Filter displayed as an image. (c) Filter radial cross section.

Basics of image processing: Fourier reject filters of images

RS FS

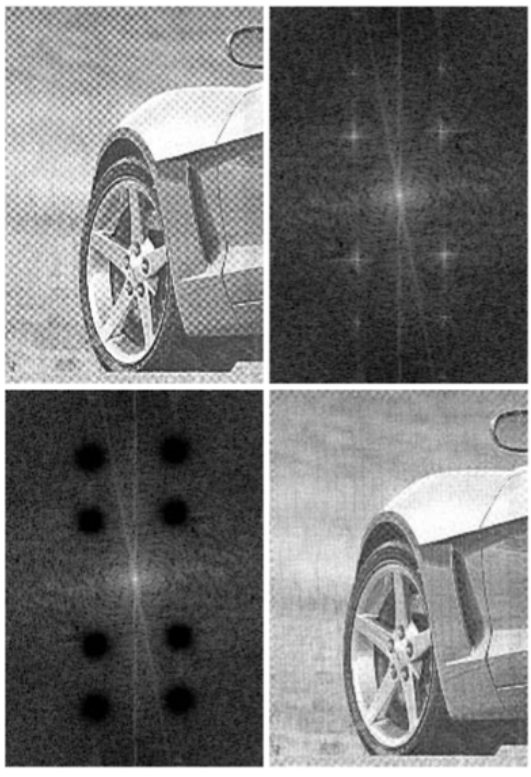

Filter Result

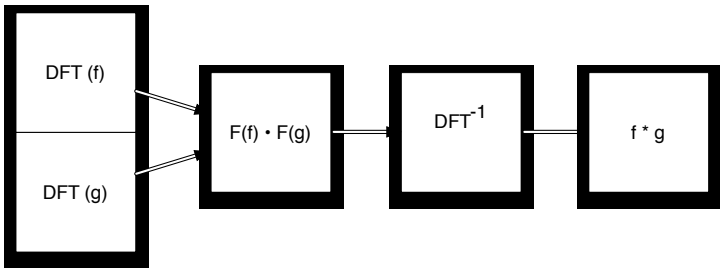

Gonzales and Woods, Digital Image Processing, 2008

Convolution

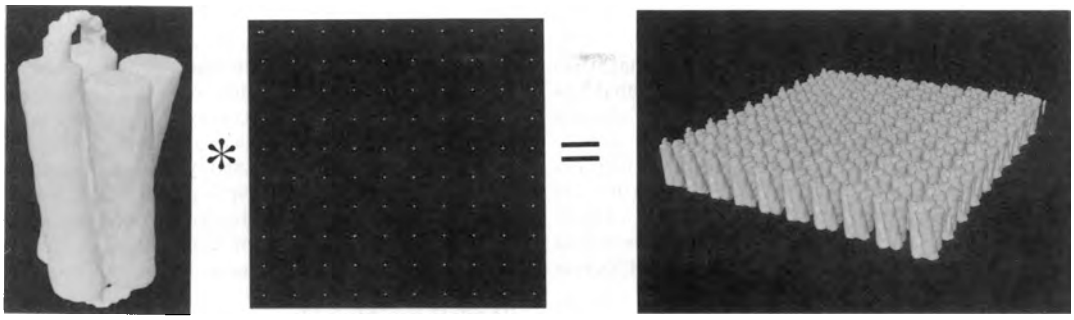

FIGURE 4 A two-dimensional crystal can be described as a convolution of an asymmetric unit and a two-dimensional lattice function. Here a four-cylinder molecular model represents the asymmetric unit. In a protein crystal, an asymmetric unit can be a single polypeptide or an integral multiple thereof.

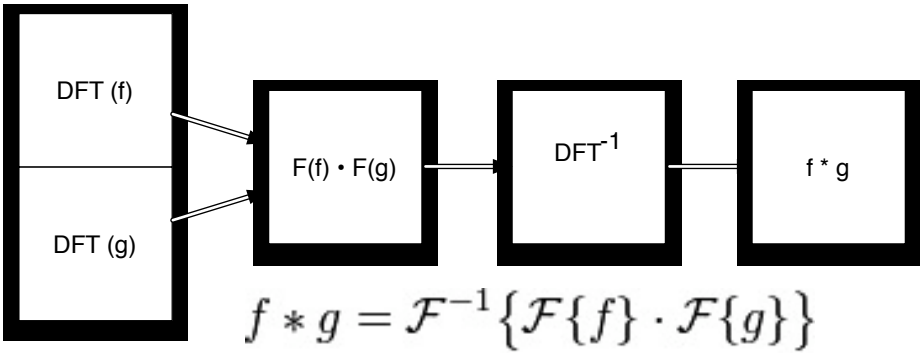

$$f * g = \mathcal{F}^{-1}\{\mathcal{F}\{f\} \cdot \mathcal{F}\{g\}\}$$

Chiu et al. Biophysical Journal (1993) vol. 64 (5) pp. 1610-25

2D crystals give rise to discontinuous diffraction patterns but they have continuous lattice lines in 3D

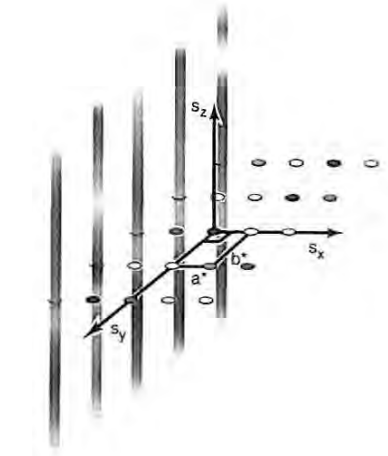

Figure 7.6 The idea of parallel lines arranged on a regular lattice in reciprocal space is shown here by a cartoon in which the lines are parallel to the s_z axis. The independent variation of the value of the Fourier transform on each line is indicated schematically by smooth variations of shading along each line. Only five such parallel lines are shown here, but the positions of others are indicated by variously shaded disks where the lines intersect the s_x, s_y plane. The parallel lines are separated from one another by fixed amounts, which can be different in two independent directions. In this particular example, the lattice is shown as being one with a 90° angle between the **a*** and **b*** basis vectors.

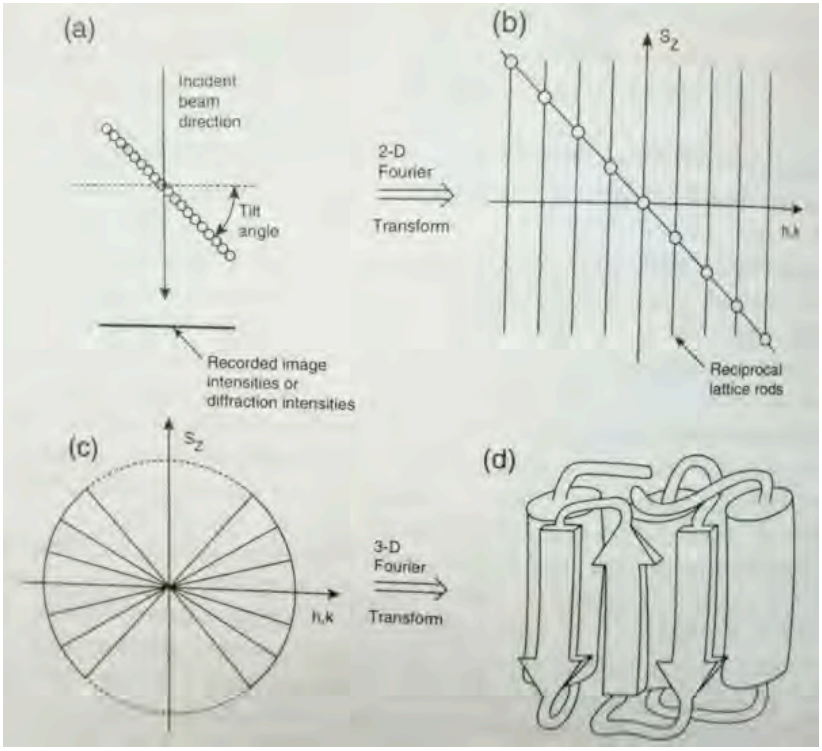

R. Glaeser. Electron Crystallography of Biological Macromolecules - Chapter 7. (2007)

Correlation

Cross correlation function

$$\frac{\sum_{i,j} f_{x+i,y+j} \cdot g_{i,j}}{\sqrt{\sum_{i,j} f^2_{x+i,y+i} \cdot \sum g^2_{i,j}}}$$

Example

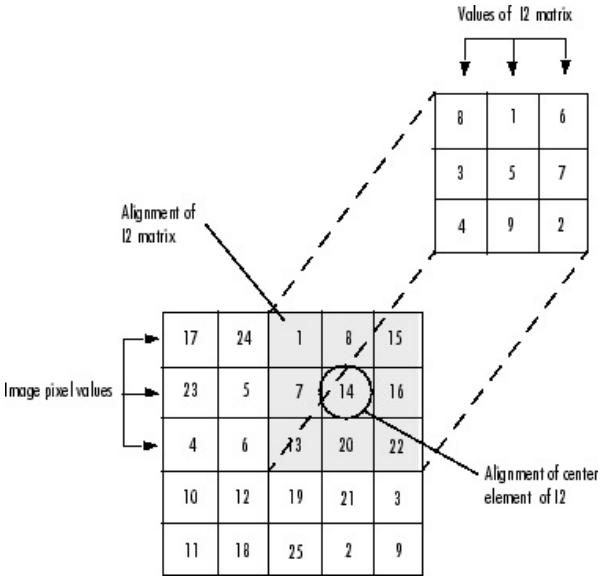

$1 \cdot 8 + 8 \cdot 1 + 15 \cdot 6 + 7 \cdot 3 + 14 \cdot 5 + 16 \cdot 7 + 13 \cdot 4 + 20 \cdot 9 + 22 \cdot 2 = 585$

Cross correlation of f and g

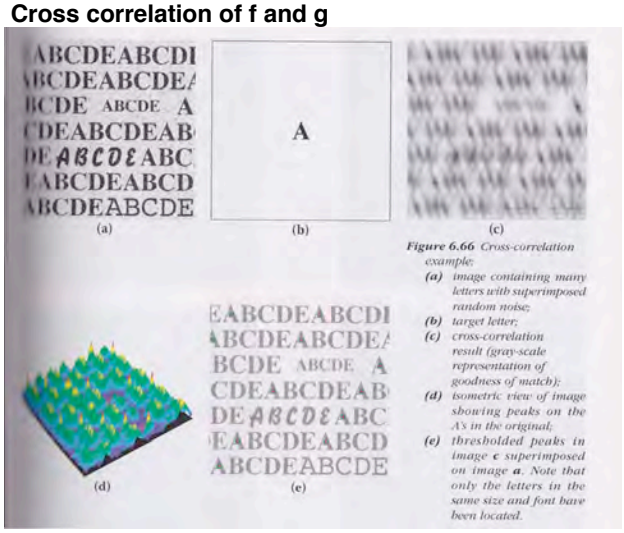

Autocorrelation function

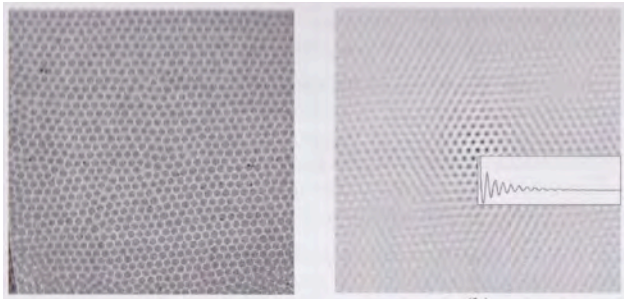

Russ, The Image Processing Handbook, 2007

Correlation

Cross correlation function

$$\frac{\sum_{i,j} f_{x+i,y+j} \cdot g_{i,j}}{\sqrt{\sum_{i,j} f^2_{x+i,y+i} \cdot \sum g^2_{i,j}}}$$

Example

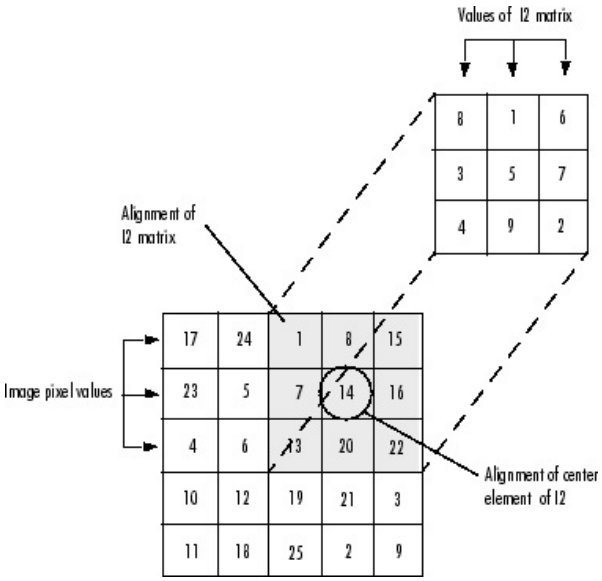

$1 \cdot 8 + 8 \cdot 1 + 15 \cdot 6 + 7 \cdot 3 + 14 \cdot 5 + 16 \cdot 7 + 13 \cdot 4 + 20 \cdot 9 + 22 \cdot 2 = 585$

Cross correlation of f and g

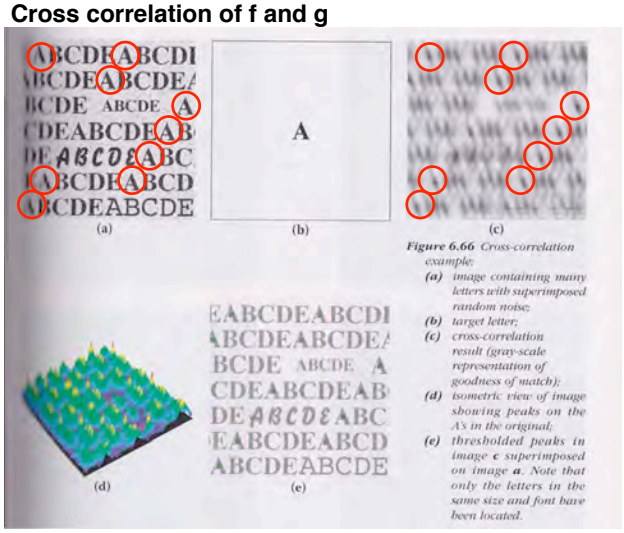

Autocorrelation function

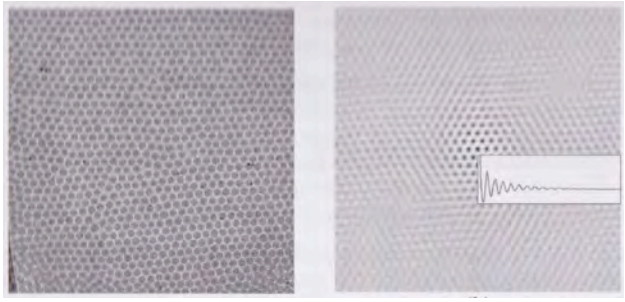

Russ, The Image Processing Handbook, 2007

Fourier theory 2D

- Basics of image processing

  Real space, Fourier space, convolution, lattice lines, correlation, autocorrelation

- Image formation

  Contrast transfer function and application

Quantitative electron cryo-microscopy: from atoms to an EM image

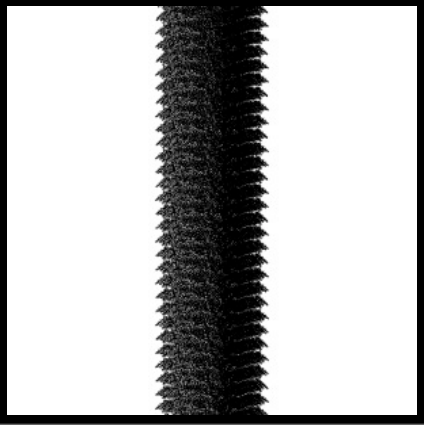

Electron microscope

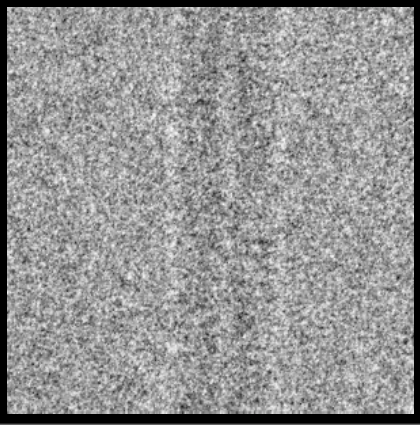

Cryo-EM images are recorded in underfocus

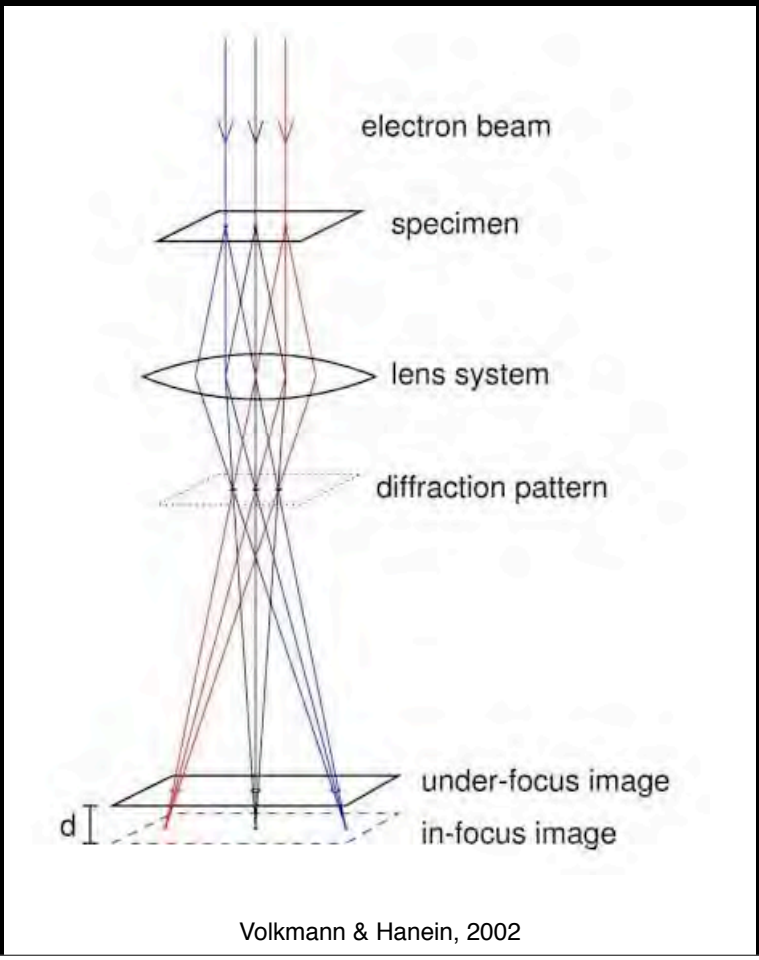

Volkmann & Hanein, 2002

Prediction of angular distribution of elastic scattering

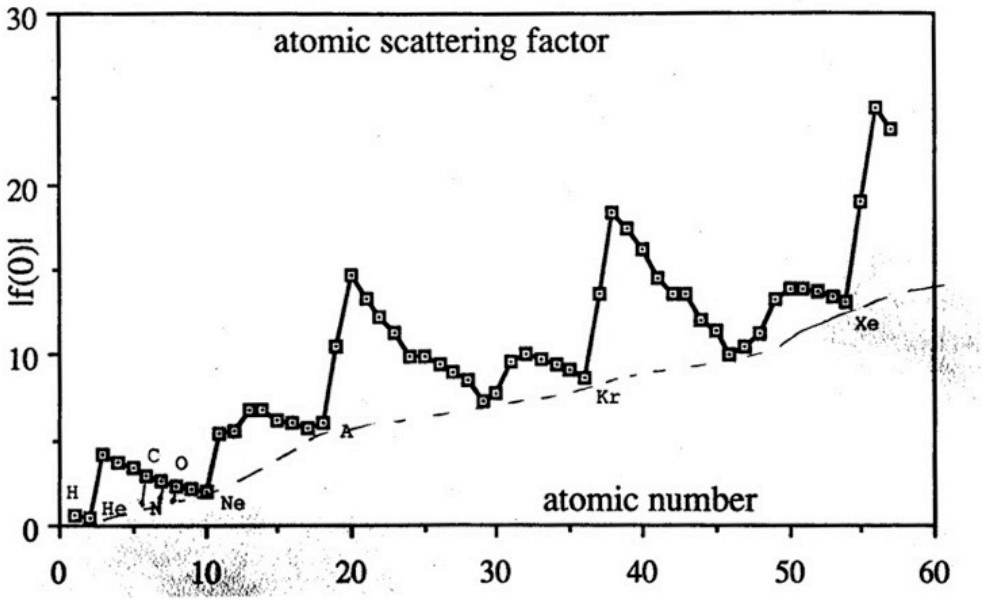

Atomic number	σ_e (pm^2) (PW)
1	3.65
6	79.4
7	85.1
8	90.4
11	148
12	187
15	314
53	1730
74	2120
79	2110
80	2160

Voltage (keV)	$Z = 6$ σ_e (pm^2) (partial wave)
10	618
40	170
70	105
100	79.4

1. Structure factors increase with atomic number Z at slope of $Z^{3/4}$ (higher contrast)
2. Elastic scattering cross section σ(e) decreases with increasing electron voltage (lower contrast)

Henderson

Langmore & Smith, Ultramicroscopy 1992

Scattering from biological molecules depends on the ice thickness

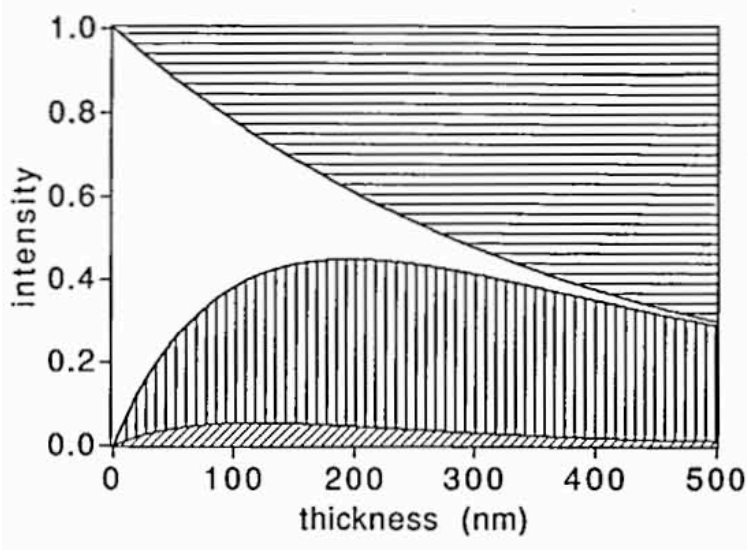

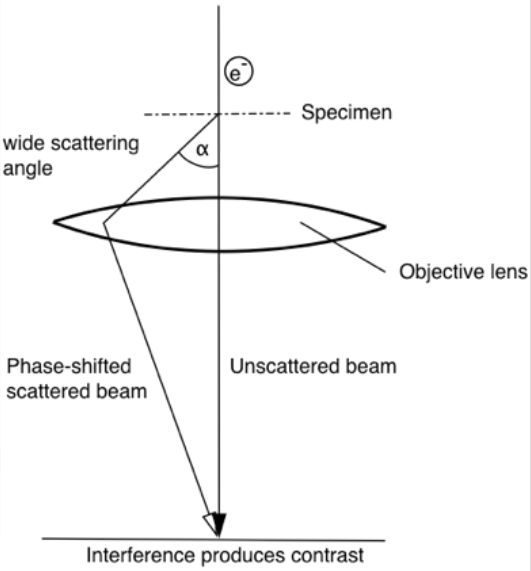

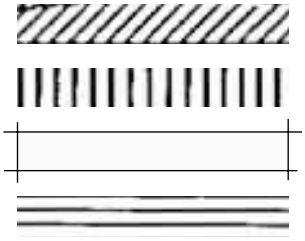

Elastic scattering within aperture

Inelastic scattering within aperture

Unscattered electrons

Scattered outside the aperture

Langmore & Smith, Ultramicroscopy 1992

1966: Thon rings

Overfocus +350 nm...Focus ...-450 nm Underfocus

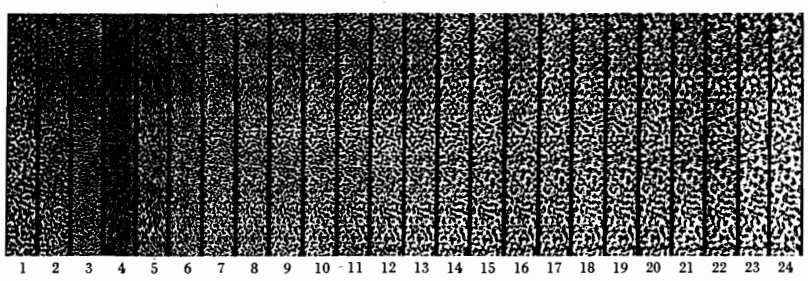

Abb. 2. Ausschnitte aus den Aufnahmen einer Fokussierungsreihe an einer dünnen Kohlefolie. Die Defokussierungswerte sind in Abb. 1 angegeben. Aufnahmedaten: $\lambda = 3{,}7 \cdot 10^{-9}$ mm (100 kV); Bestrahlungsapertur $\alpha_B \approx 1 \cdot 10^{-3}$; Objektivapertur $\alpha_0 = 9{,}6 \cdot 10^{-3}$; elektronenoptische Vergrößerung 178 000 : 1; Gesamtvergrößerung 620 000 : 1.

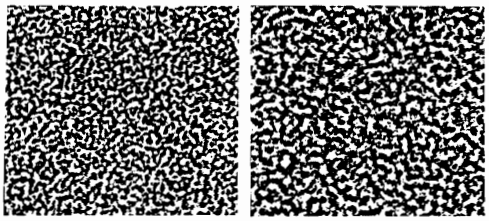

Abb. 3. $\Delta z = +110$ nm. Abb. 4. $\Delta z = +230$ nm.

Abb. 3 und 4. Bildstrukturen bei Defokussierungswerten Δz in der Nähe der Scheitel S_0 und S_{-1}. Gesamtvergrößerung 1 500 000 : 1.

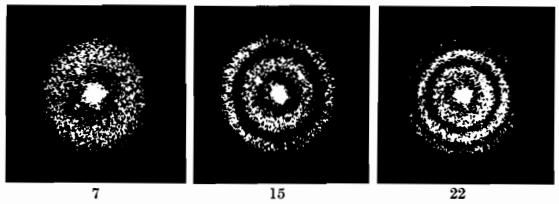

Abb. 6. Lichtoptische Beugungsfiguren, die an den Bildstrukturen der Aufnahmen 7, 15 und 22 der Fokussierungsreihe (Abb. 2) mittels der in Abb. 5 beschriebenen Anordnung gewonnen wurden.

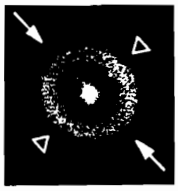

Abb. 8. Elliptische Beugungsfigur leicht astigmatischer Bildstrukturen. Dem Abstand der Pfeilspitzen entspricht $\Delta 1 = 0{,}58$ nm, dem Abstand der Dreieckspitzen $\Delta 1 = 0{,}67$ nm.

Thon, Zeitschrift Naturforschung 1966

Astigmatism detectable from Thon rings

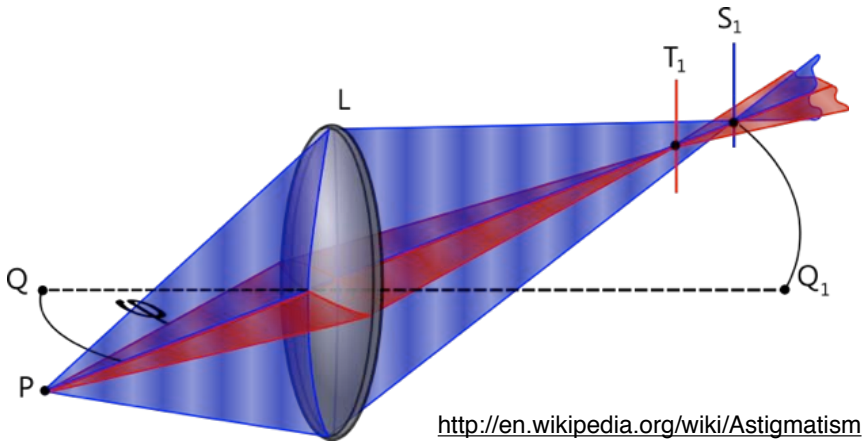

http://en.wikipedia.org/wiki/Astigmatism

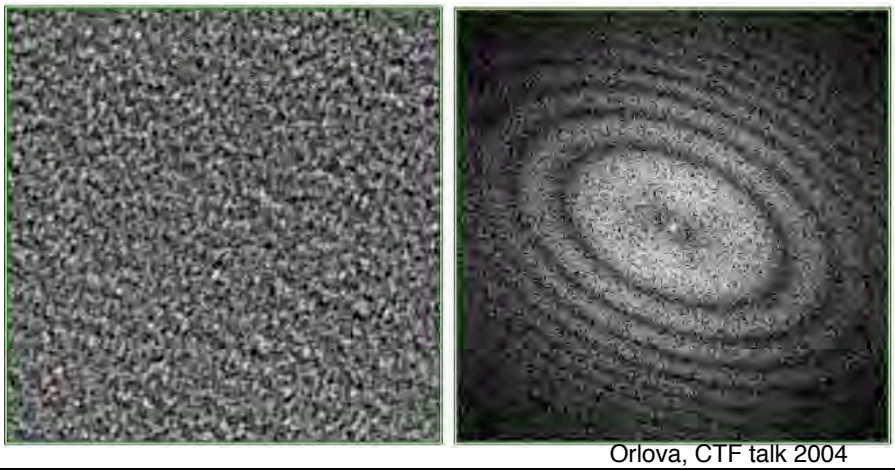

Orlova, CTF talk 2004

Drift detectable from Thon rings

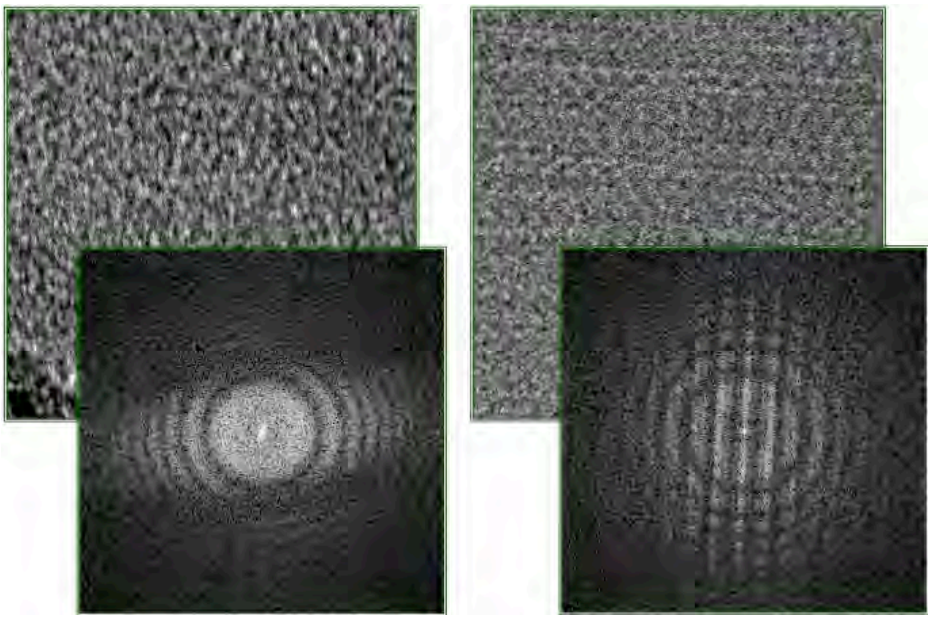

Orlova, CTF talk 2004

1970: Erickson & Klug

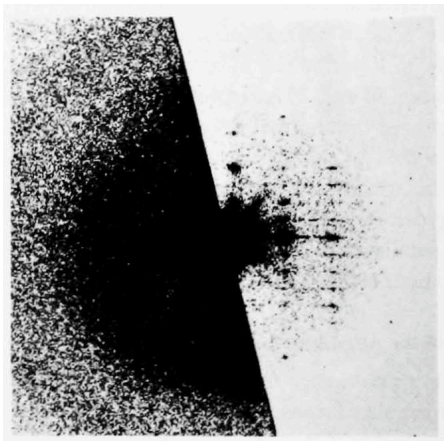

Erickson & Klug, Bericht Bunsengesellschaft 1970

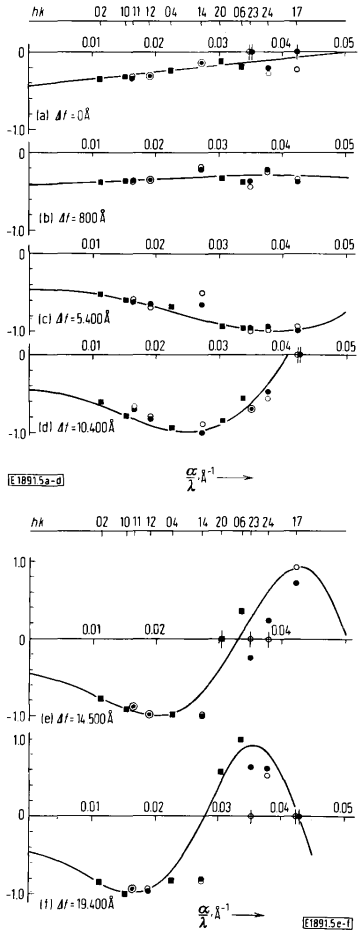

Contrast-transfer theory

Object transform

Microscope CTF

$$T^{i}_{Ob}(\alpha,\phi) = -T^{0}(\alpha,\phi)\,f(\alpha)\,A(\alpha)\,[\sin\chi(\alpha) + Q(\alpha)\cos\chi(\alpha)].$$

$$\mathrm{CTF} = [\sin\chi(\alpha) + Q(\alpha)\cos\chi(\alpha)],$$

Scattering angle α

χ - phase shift due to:

λ - wavelength of electrons

C_s - spherical aberration

Δ*f* - defocus

$$\chi(\alpha) = \frac{2\pi}{\lambda}\left[-C_s\frac{\alpha^4}{4} + \Delta f\,\frac{\alpha^2}{2}\right] \qquad (2)$$

where C_s is the coefficient of spherical aberration and Δf is the defocussing (positive for a weak or underfocussed lens).

Q - amplitude contrast ratio

Q ~ 7-14 % for biological specimens in ice

Q ~ 15-35 % for biological specimens in Uranyl Acetate

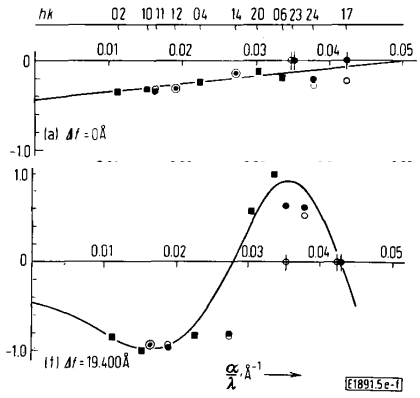

Erickson & Klug, Bericht Bunsengesellschaft 1970

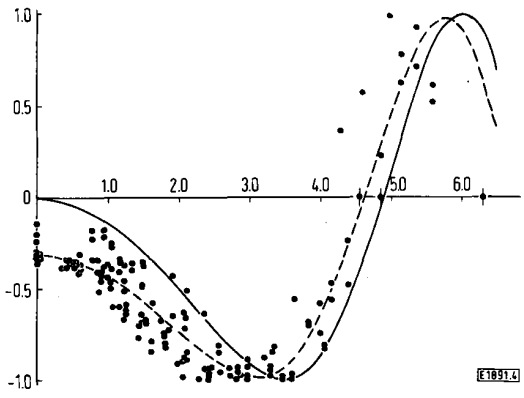

Fig. 4

Scaled amplitudes from the complete focal series plotted as a function of the common variable $u = \alpha/\lambda\sqrt{\Delta f}$. The solid curve is the theoretical transfer function for the case of pure phase contrast, $-\sin\pi\lambda u^2$. The dashed curve is the theoretical transfer function assuming 35 per cent amplitude contrast, $-[.93\sin\pi\lambda u^2 + .35\cos\pi\lambda u^2]$

Contrast Transfer Function

CTF

Non-tilted sample

Resolution
(1 / Å)

Image

Stahlberg, CTF talk 2006

Contrast Transfer Function

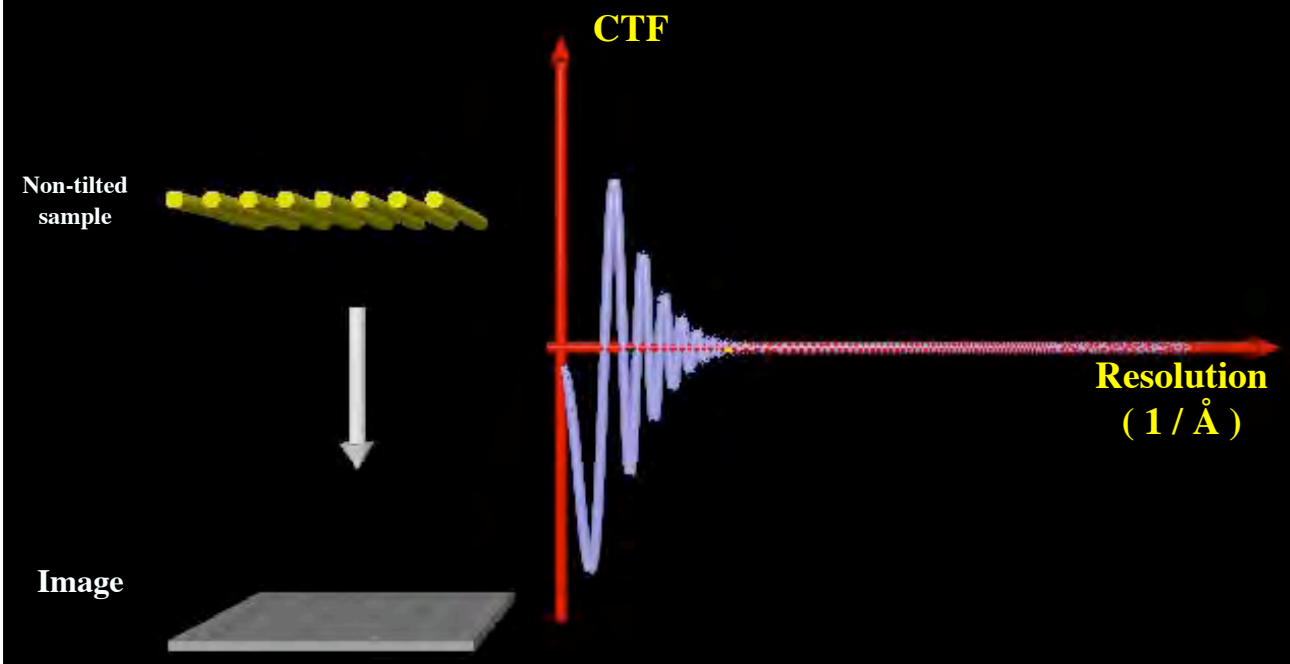

Stahlberg, CTF talk 2006

Cryo-EM images are under focussed

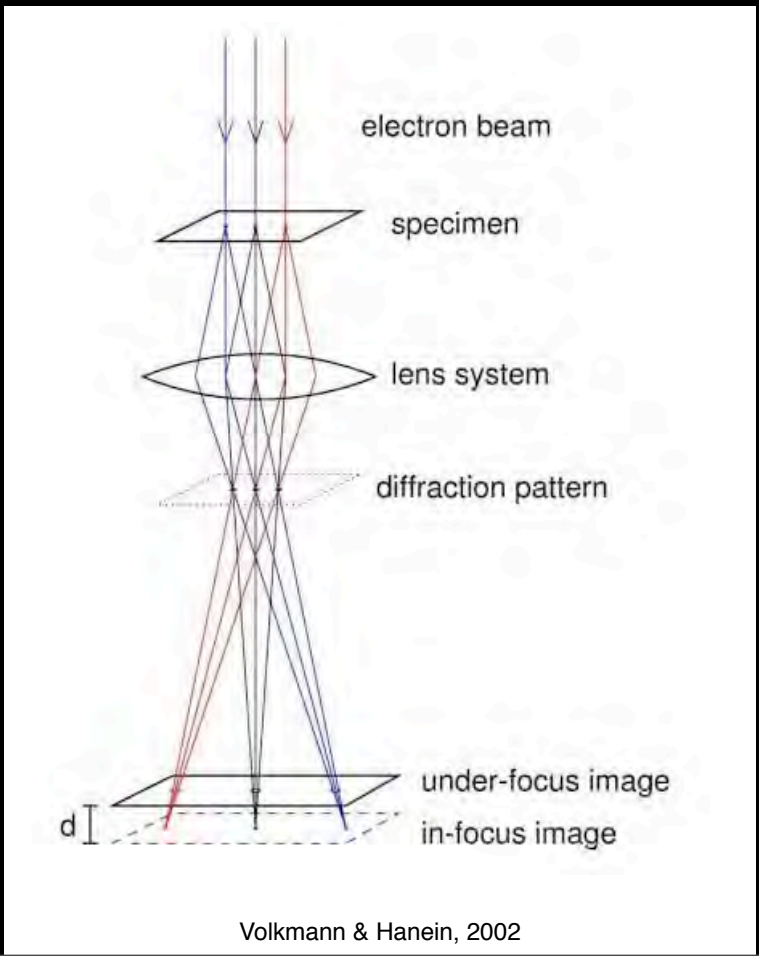

Volkmann & Hanein, 2002

Influence of defocus on a single point: point-spread function

Δf = 80 nm

Δf = 600 nm

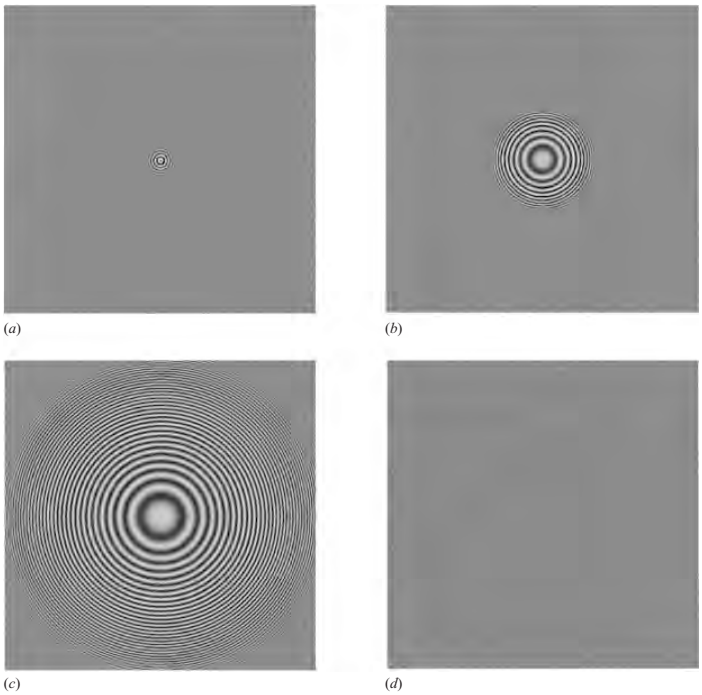

Δf = 1500 nm

compensated by phase flipping

Fig. 2. Extent of the point spread function (PSF) in real space. The PSF is the Fourier transform of the CTF and represents an alternative way of describing the same concept. The PSF, at defocus values that are typically used in cryo-EM, lead to a spread of the information of a single 1 Å 'pixel' of the image (256 × 256 pixels), over an area as large as an *E. coli* ribosome. The defocus values used here, in part correspond to the CM300 defocus values used in Fig. 1. The calculations were performed with the 'Impose CTF' option of the IMAGIC TRANSFER program (see main text). (*a*) PSF of the CM300 at 1·1 Scherzer (~ 800 Å underfocus). (*b*) PSF CM300 at 9 Scherzer (6000 Å underfocus). (*c*) PSF CM300 at ~ 23 Scherzer (1·5 µm underfocus). (*d*) PSF CM300 at 9 Scherzer (6000 Å underfocus) after CTF correction by phase flipping.

van Heel et al., Q Rev Biophys 2000

Influence of defocus on 2D image

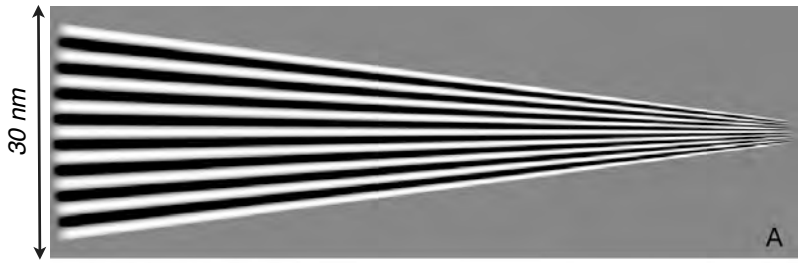

Δf = 0 nm

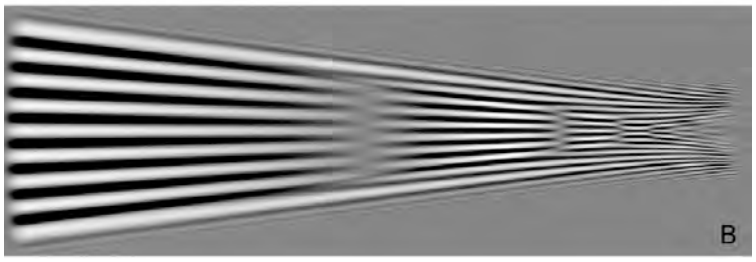

Δf = 2000 nm

Downing & Glaeser, Ultramicroscopy 2008

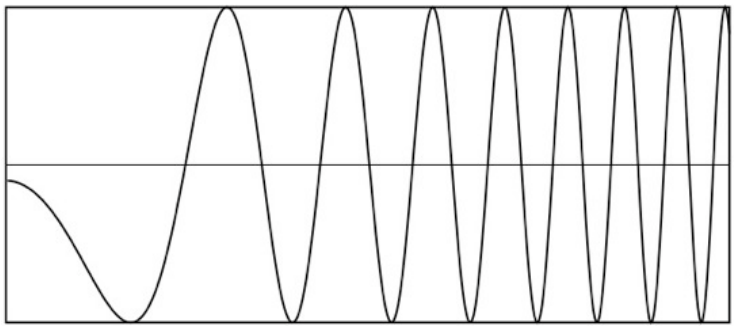

The influence of defocus on a 1D image

1D profile through projection of TMV

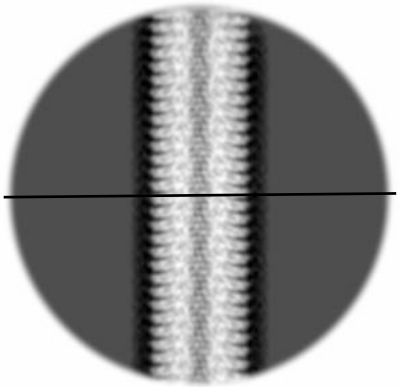

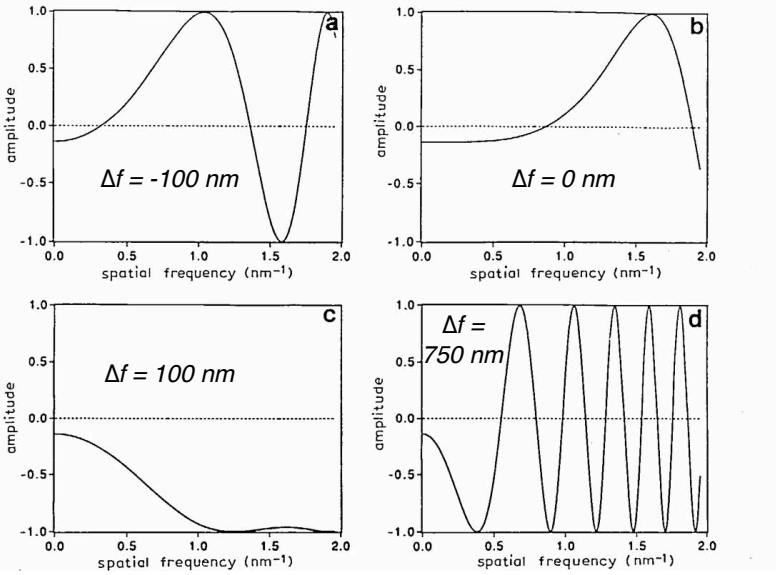

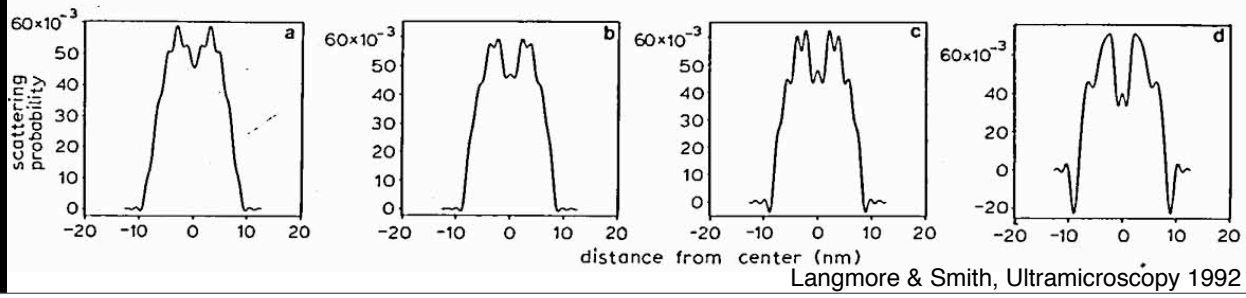

Langmore & Smith, Ultramicroscopy 1992

Compensation of CTF

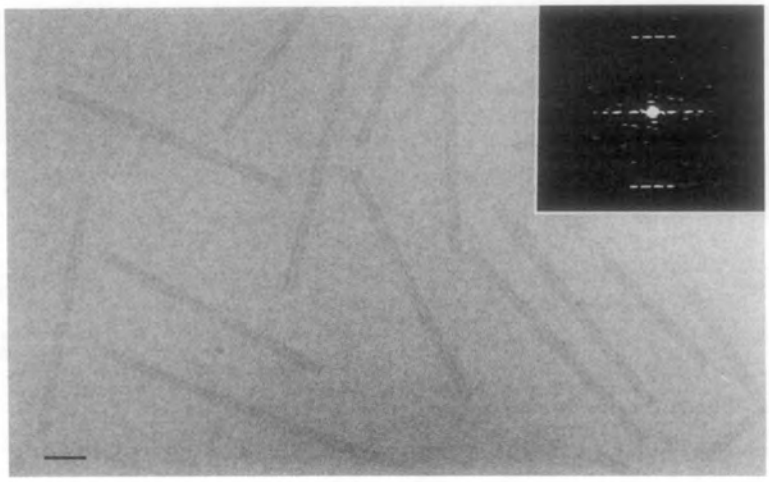

Figure 4. Low-dose bright-field image of energy-filtered frozen-hydrated TMV at 780 nm defocus. Inset is a calculated Fourier transform of a 100 nm segment of TMV. The bar represents 50 nm.

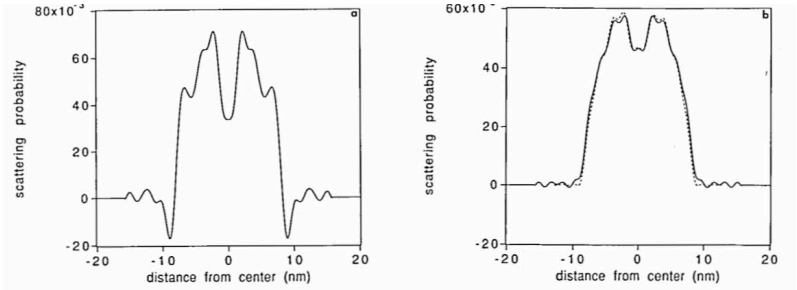

Fig. 13. Effects of CTF compensation on projections of frozen-hydrated TMV. (a) Observed scattering probabilities of TMV at 780 nm defocus. (b) Comparison of the observed scattering probabilities after CTF compensation (———), and the predicted scattering probabilities (------). 1.9 nm resolution. From ref. [37].

$\Delta f = 780$ nm compensated

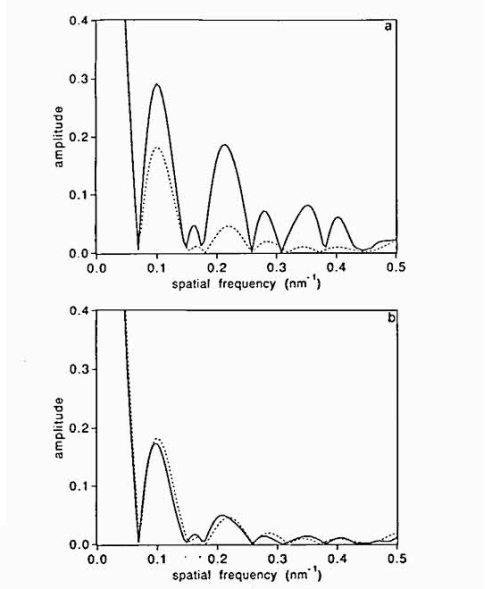

Fig. 12. Observed and predicted one-dimensional Fourier equatorial transforms of frozen-hydrated TMV. (a) Fourier transform of the observed image with 780 nm defocus (———); Fourier transform of the predicted scattering from TMV (------). (b) Fourier transform of the observed image after CTF compensation (———); Fourier transform of the predicted scattering from TMV (------). Comparison of the observed and predicted Fourier amplitudes gave a crystallographic R factor of 0.12, where $R = \Sigma|F_{obs} - F_{pred}|/\Sigma F_{obs}$. CTFs were calculated assuming $Q = 0.14$. Fourier transforms were normalized to unity at zero spatial frequency. 1.9 nm resolution. Data from ref. [37].

Smith & Langmore, J Mol Biol 1992

The envelope of the CTF is significantly reduced by FEG microscopes

Table 1. Comparison of the typical parameters of a thermionic source and a FEG

	Thermionic source	Field-emission gun
Illumination aperture β	$1.6 \cdot 10^{-4}$ rad	$5 \cdot 10^{-6}$ rad
Lateral coherence width $r_c = 0.16 \cdot \lambda/\beta$	37 Å	1200 Å
Brightness b	10^6 A cm^{-2} sr^{-1}	10^9 A cm^{-2} sr^{-1}
Solid angle $\omega = 2\pi(1\text{-cos }\beta)$ $\omega \approx \pi\beta^2$	$8 \cdot 10^{-8}$ sr	$8 \cdot 10^{-11}$ sr
Current density in specimen plane $j = b \cdot \omega$	50 eÅ^{-2} sec^{-1}	50 eÅ^{-2} sec^{-1}

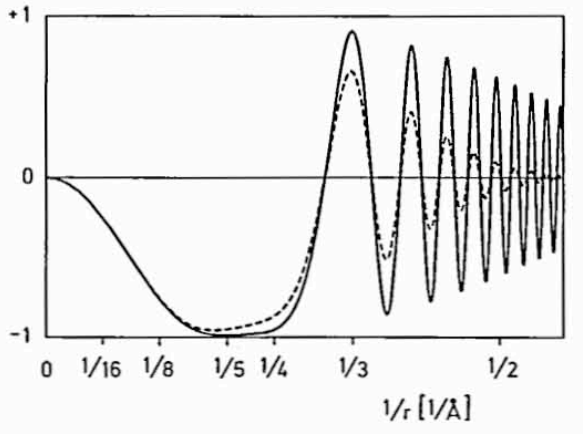

(a)

Fig. 2. Phase-contrast transfer-functions, inner curves due to thermionic source (dashed) outer curves due to field-emission gun. (a) Scherzer focus $\Delta f = \sqrt{C_s \cdot \lambda}$.

Zemlin, Micron 1994

The B-factor describes the decay of high-resolution detail

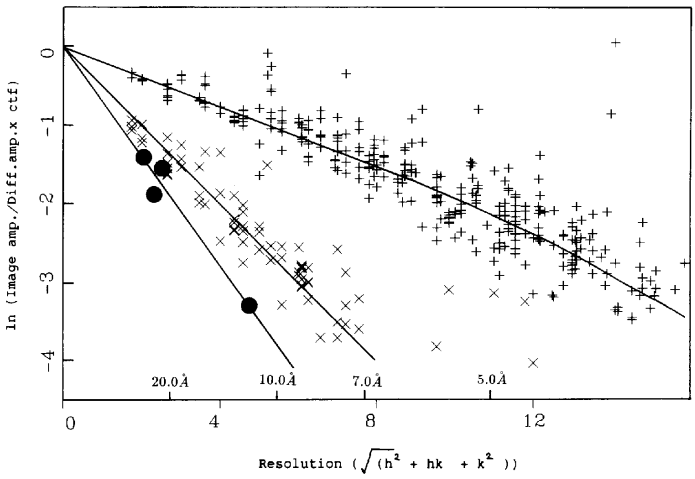

Fig. 12. Comparison of the plots of contrast versus resolution for the best TMV image (●) with similar data for the best purple membrane low temperature (+) and room temperature (×) images. It is clear that the TMV contrast falls off at considerably lower resolution, and that for this reason the purple membrane analysis has been possible to 3 Å, whereas the TMV can only be carried out at 10 Å at the present time.

Henderson, Ultramicroscopy 1992

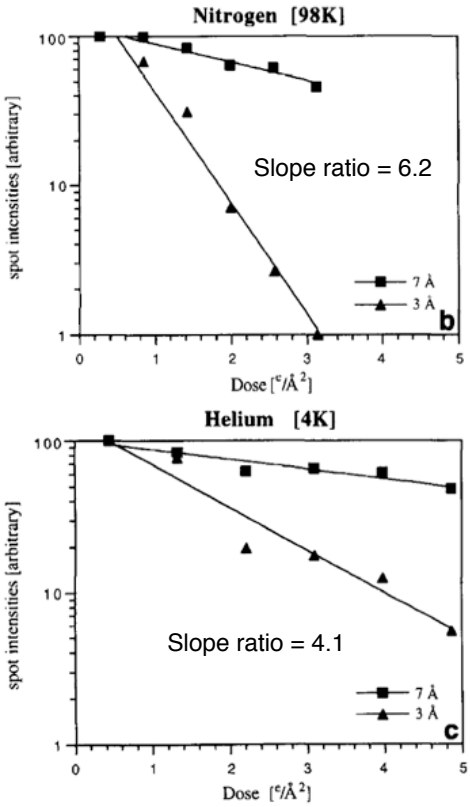

1. Radiation damage degrades structure factors ΔB = 80
2. Detectors (e.g. film) poor high resolution DQE ΔB = 60
3. Charging and mechanical movement ΔB = 60 to 500
4. Intrinsic molecular flexibility ΔB = 30 to 500

Stark, Zemlin & Boettcher (1996) Ultramicroscopy

Simulating the CTF

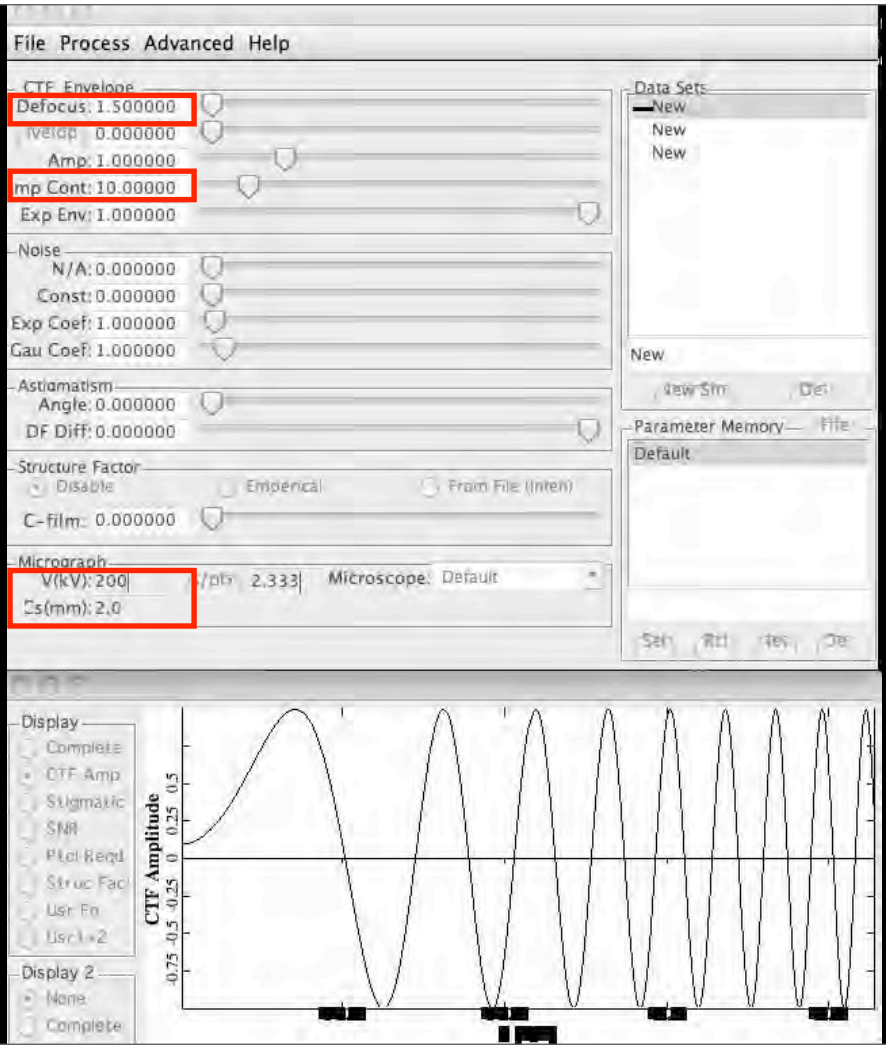

CTFIT (EMAN)

Simulating the CTF

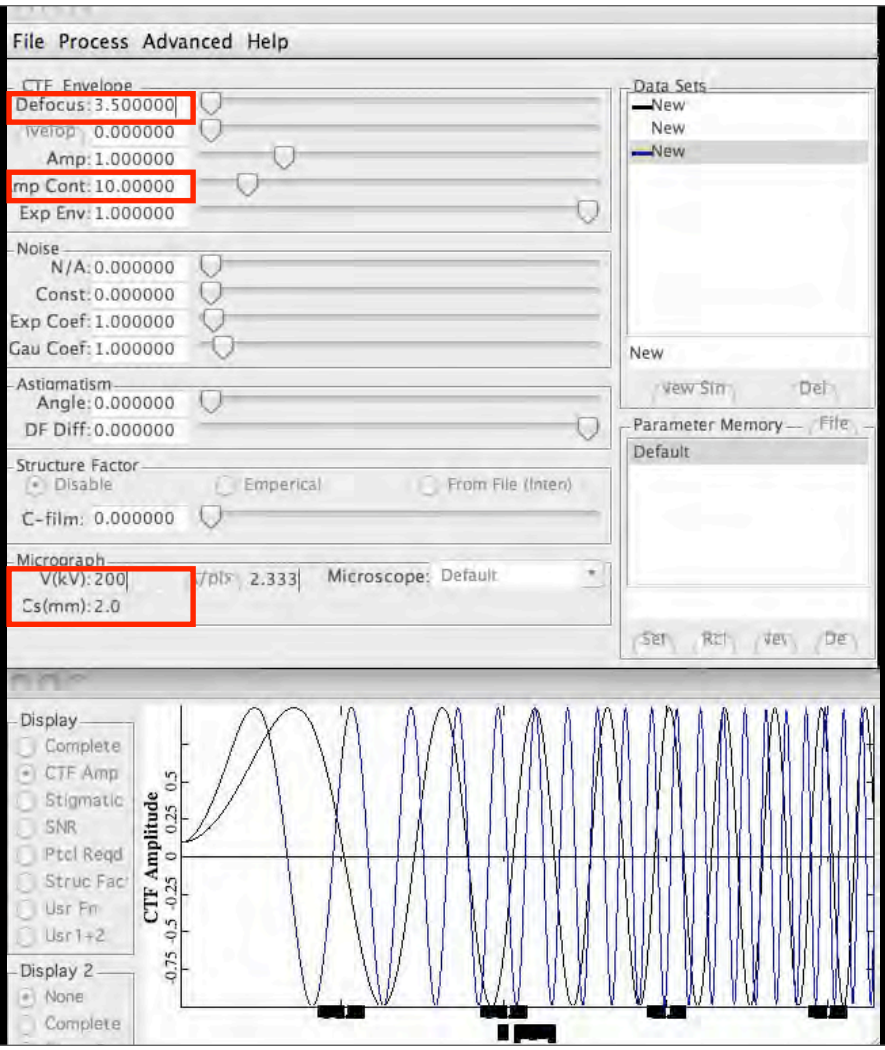

CTFIT (EMAN)

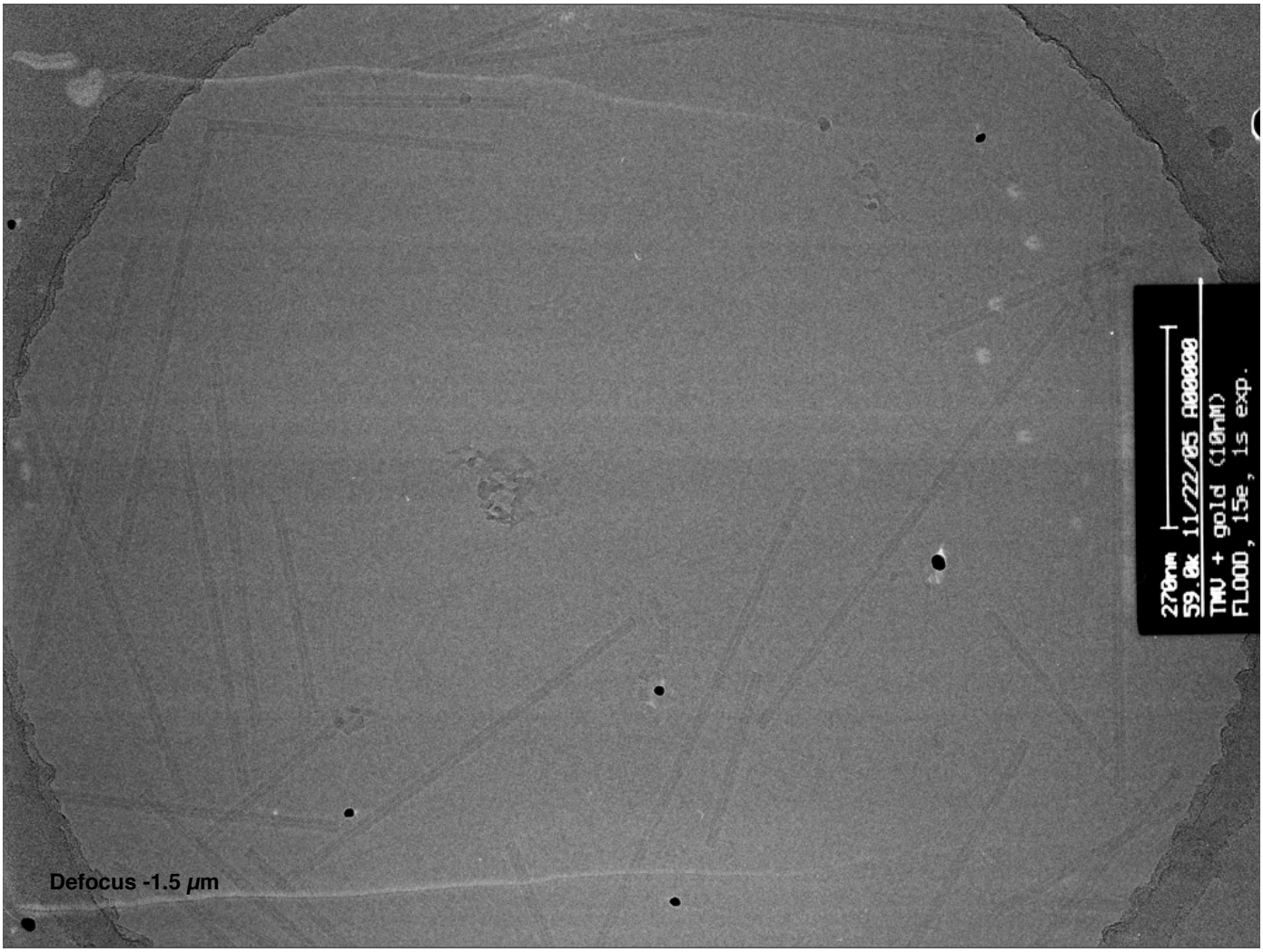

Defocus -1.5 *μm*

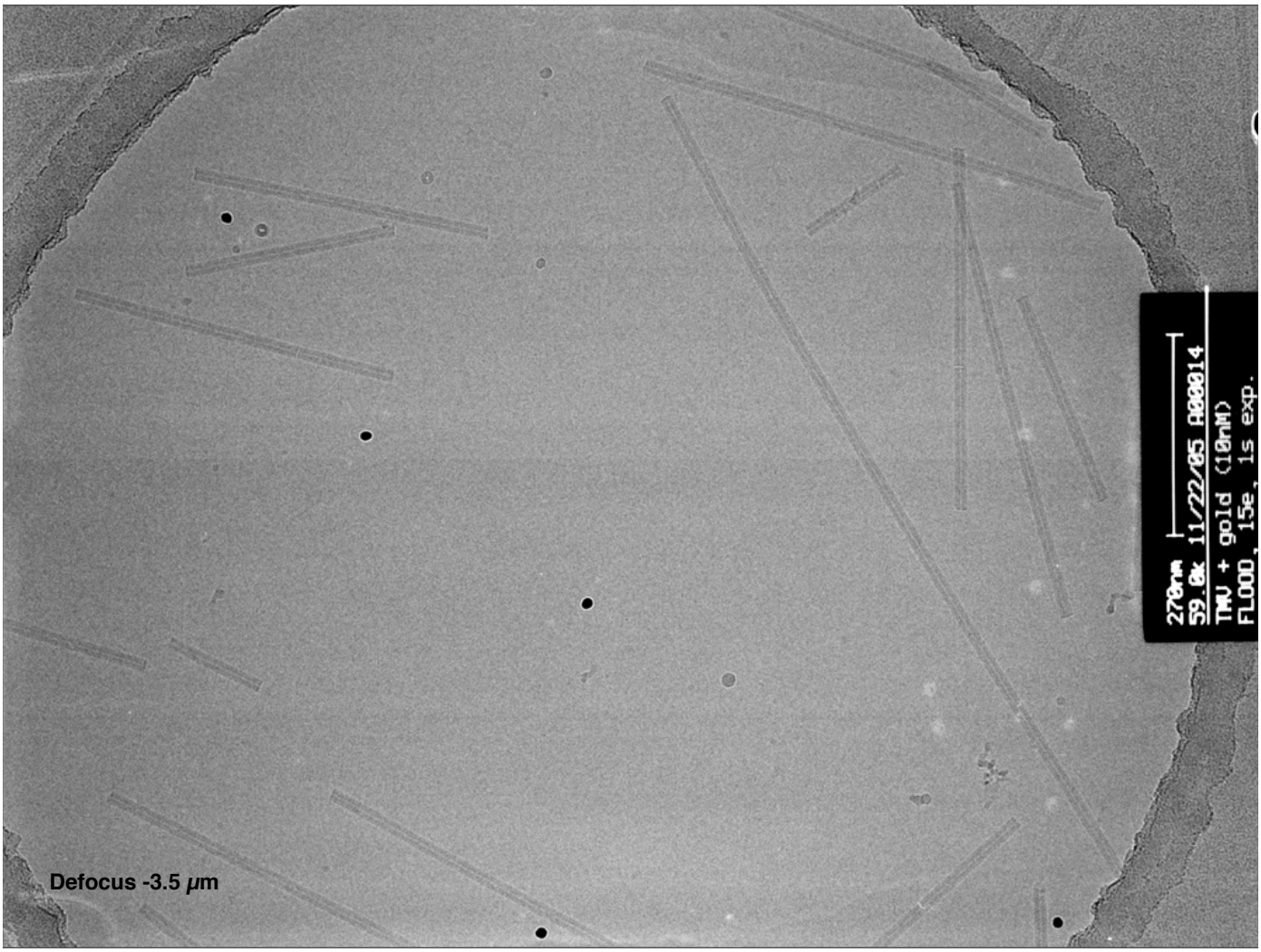

Software for CTF determination

- IMAGIC TRANSFER
- SPIDER
- EMAN - CTFIT graphical interface
- MRC programs: CTFFIND3/CTFTILT2

2D crystals: S/N weighting and phase flipping

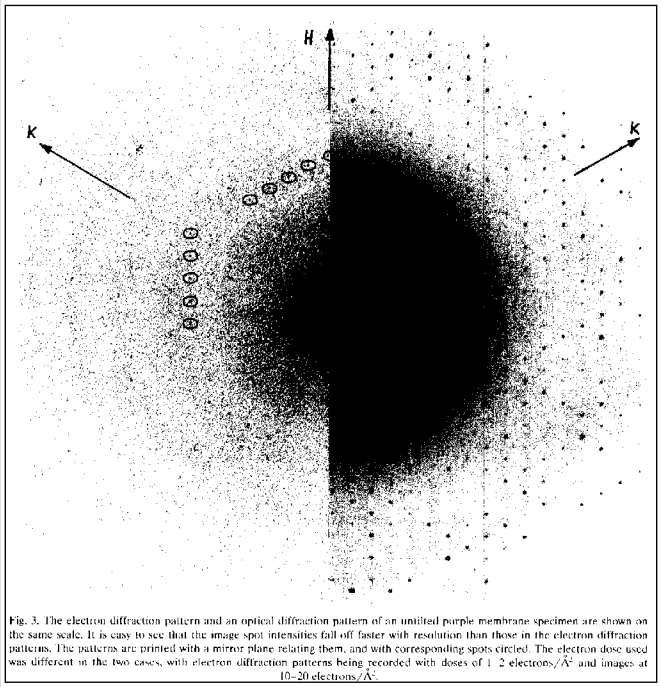

Fig. 3. The electron diffraction pattern and an optical diffraction pattern of an untilted purple membrane specimen are shown on the same scale. It is easy to see that the image spot intensities fall off faster with resolution than those in the electron diffraction patterns. The patterns are printed with a mirror plane relating them, and with corresponding spots circled. The electron dose used was different in the two cases, with electron diffraction patterns being recorded with doses of 1–2 electrons/Å^2 and images at 10–20 electrons/Å^2.

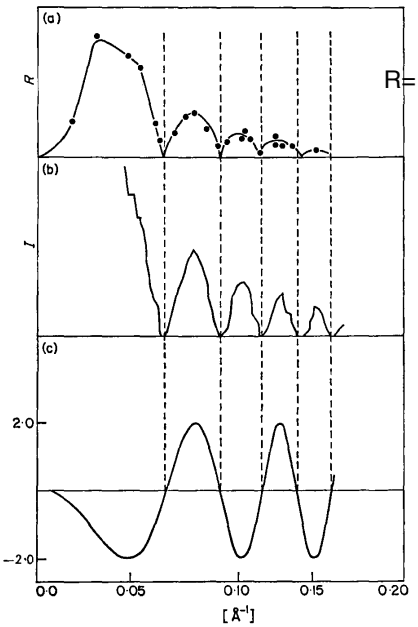

R= FT Amp.(image) / Diffraction Amp.

Intensities of FT from low-dose image

derived CTF

FIG. 2. Demonstration of the accuracy of the method of determining the signs of the phases by using information from a second micrograph. (a) The structure factor amplitudes calculated from a low-dose micrograph of the purple membrane as ratios (R) of their electron diffraction values, plotted against spatial frequency; they form a curve consisting of a series of maxima and minima. (b) The background-corrected intensity (I) across the optical transform of the corresponding high-dose micrograph; the positions of its maxima and minima match up almost exactly with those in (a). (c) The phase contrast transfer function appropriate to (b) (under-focus = 5750 Å; spherical aberration coefficient = 1·6 mm), illustrating how the sign assignments are made.

Henderson, Ultramicroscopy 1992

Henderson & Unwin, J Mol Biol 1975

SPIDER for CTF determination

1. Estimation of the defocus of each micrograph from its averaged power spectrum

2. Interactive determination of the defocus of each micrograph

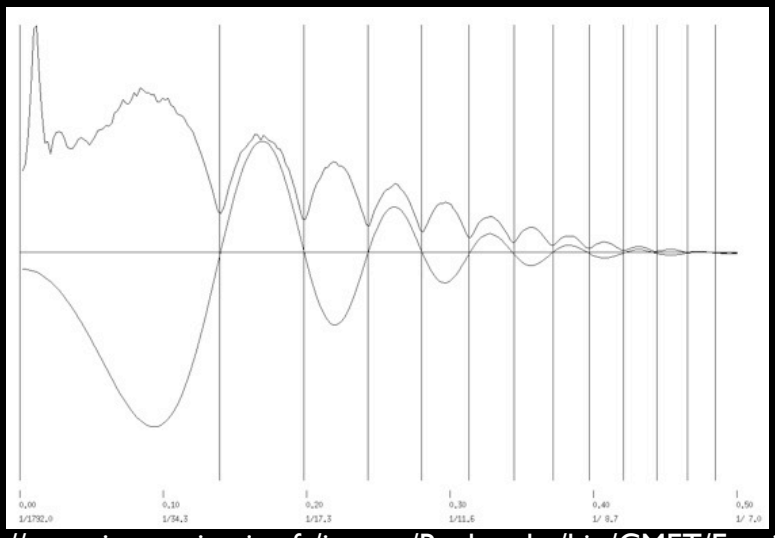

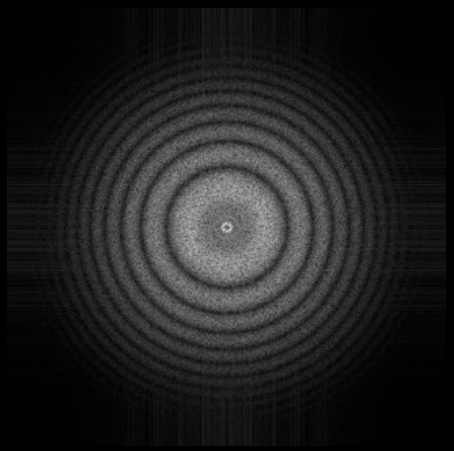

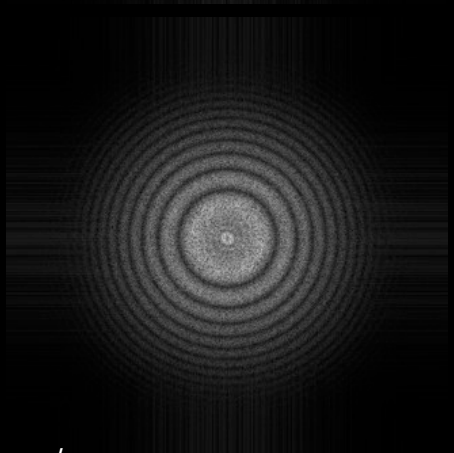

http://www.impmc.jussieu.fr/impmc/Recherche/bio/CMET/Enseignement/

CTFFIND3 determines CTF incl. astigmatism

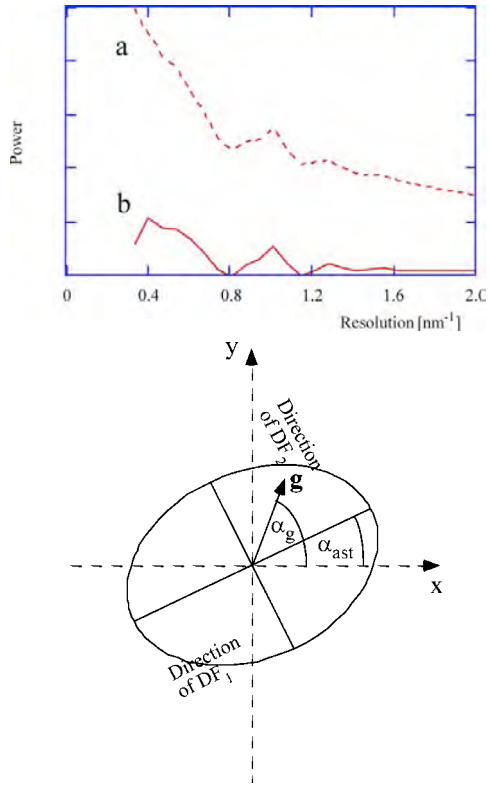

Fig. 3. Definitions for the CTF parameters DF_1, DF_2, and α_{ast}. The angle α_g of the scattering vector $\boldsymbol{g} = \boldsymbol{k}' - \boldsymbol{k}$ ($\boldsymbol{k}$, wave vector of the incident wave; $\boldsymbol{k}'$, wave vector of the scattered wave) is used in Eq. (6), indicating the point where the CTF is evaluated.

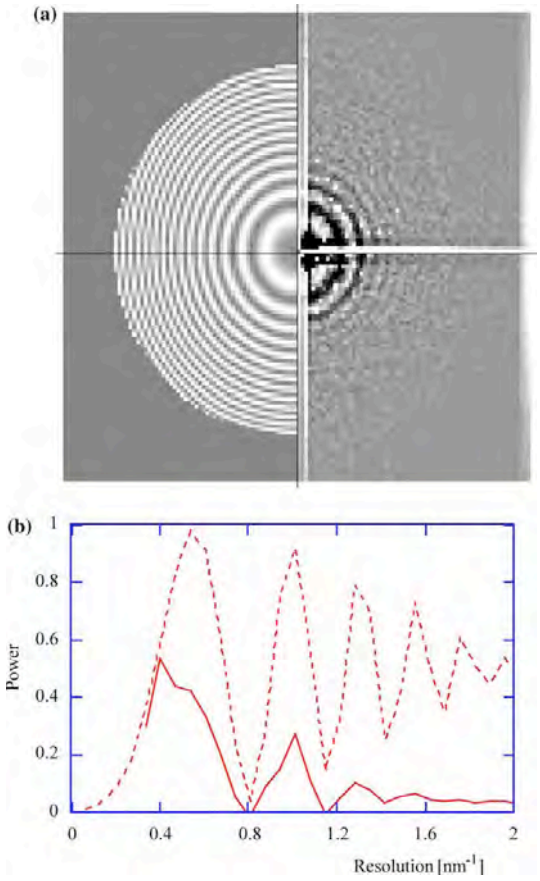

Mindell & Grigorieff, J Struct Biol 2003

Defocus gradient across the micrograph

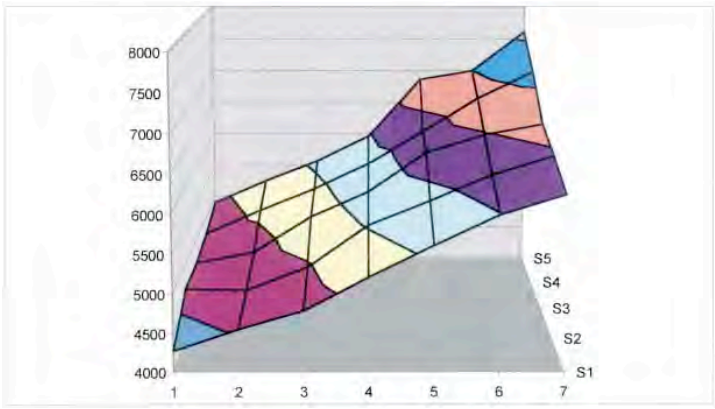

Fig. 6. Position dependent PhCTF determination. This graph illustrates a typical nominal '0' tilt on our CM200 cryo-EM/Gatan cryo-holder system. The system exhibits a systematic 6° tilt with respect to the nominal tilt angles that, if not corrected for, causes a defocus spread of almost 3000 Å. After our diagnostic analysis, the holder is now systematically used at a nominal −6° tilt to compensate for this effect. However, the defocus difference between front and back of the plot of ~ 600 Å – perpendicular to the tilt axis of the goniometer – is not correctable with the current set up. Moreover, due to a recent repair of this particular holder, the nominal '0°' tilt position requires recalibration.

van Heel et al., Q Rev Biophys 2000

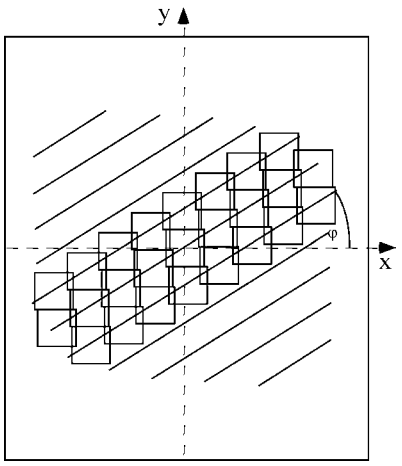

Fig. 5. Determination of tilt axis. Power spectra are calculated for each tile along the eleven parallel lines (tiles are only indicated for the three central lines). The angle φ is searched in 2° steps to find the direction in which the variance between the power spectra is minimized.

CTFTILT

Mindell & Grigorieff, J Struct Biol 2003

Methods of CTF-correction

2D crystals

- (S/N weighting and phase flipping)

Single particles

- Phase flipping
- CTF multiplication
- Wiener filtering of 3D volumes (Böttcher et al. 1997, Penczek et al., 1997)
- Image multiplication by CTF and Wiener filtration of 3D volume (Grigorieff 1998, Sachse et al. 2007)

Phase flipping vs. CTF multiplication

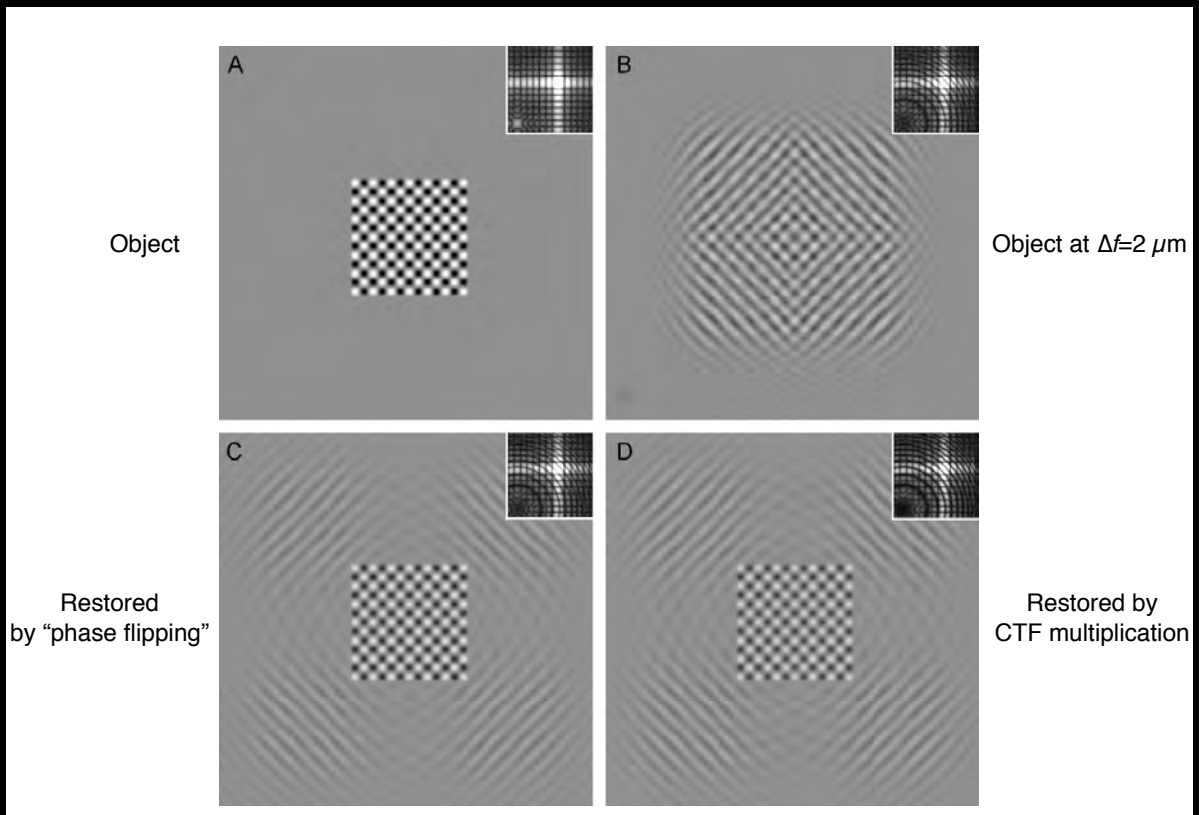

Fig. 2. Comparison of the restoration of delocalized information that is achieved by phase flipping and by multiplication by the CTF. (A) A spatially bounded cross-grating pattern is formed as the product of two perpendicular sine waves. With the size-scale set to 0.1 nm per pixel, the period is 1.3 nm. (B) The image of the object in (A) that is computed with an effective defocus of 2 μm. (C) Restoration of (B) obtained by "phase flipping"—i.e. inverting the sign of the Fourier transform of (B) in alternate zones of the CTF. (D) Restoration of (B) computed by multiplying the Fourier transform by the original CTF. Insets show a section of the Fourier transform, with the origin near the lower left corner.

Downing & Glaeser, Ultramicroscopy 2008

Wiener filter

$$F(k) = \frac{H^*(k)}{|H(k)|^2 + 1/SNR}$$

1. no noise SNR -->infinity

2. pure noise SNR -->0

$$F_{ps}(k) = \begin{cases} \dfrac{1}{H(k)} & H(k) \neq 0 \\ \text{for} & \\ 0 & H(k) = 0 \end{cases}$$

Penzcek et al., Scanning Microscopy 1997

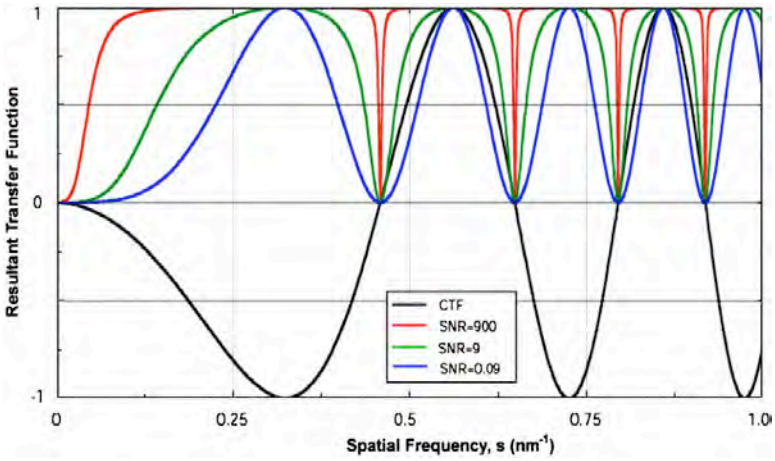

Fig. 4. The phase-contrast CTF for a defocus of 2 μm and electron energy of 300 keV, and the weighting (resultant "transfer function") that is provided when a Weiner filter is used for image restoration. The CTF is shown by the black curve, while the product of the CTF and the Wiener filter is shown as differently colored curves for which the value of the SNR is identified in the insert. See the text for further explanation.

Downing & Glaeser, Ultramicroscopy 2008

Fourier transforms according to David DeRosier

What you see.	What you get
Spots	Excited
Spot positions	Unit cell size and shape
Spot size	Size of coherent domains
Intensity relative to background	Signal/noise ratio
Distance to farthest spot	Resolution
Amplitude and phases of spots	Structure of molecules
Positions of Thon rings	Amount of defocus
Ellipticity of Thon rings	Amount of astigmatism
Asymmetric intensity of Thon rings	Amount of instability
Direction of asymmetry	Direction of instability